10
Green Nanofabrication: Unconventional Approaches for the Conservative Use of Energy

Darren J. Lipomi, Emily A. Weiss, and George M. Whitesides

10.1
Introduction

Many of the chapters in this book describe the ways that nanostructured materials contribute to the conversion and storage of energy. The goal of this chapter is to highlight strategies that make efficient use of energy[1)] for the production of the nanostructures themselves ("green nanofabrication"). We define nanofabrication as the collection of methods that generates structures with sizes of less than 100 nm in at least one dimension [1]. By this definition, nanostructures have been fabricated as components of microelectronic devices for about a decade. Microprocessors are fabricated by high-performance techniques in facilities with rigorous environmental controls. These techniques – which we refer to as "conventional techniques" – make information technology possible and will not be replaced in the foreseeable future. They are, however, intensive consumers of energy and natural resources. Many emerging applications of nanotechnology – in optics, sensing, separations, biology and photovoltaics – tend to be more defect-tolerant than are microchips. Conventional techniques often are capable of producing structures for such defect-tolerant applications, but the sacrifice of efficiency (and cost) for precision made by conventional methods is, at best, unnecessary and, at worst, unacceptable.

Real and potential applications of nanotechnology pervade almost every branch of science and engineering. This book is concerned with applications of nanotechnology for energy, but comparably important applications exist in biology, chemistry, medicine, materials and the field in which it already enjoys the most success – information technology. As industrial and governmental spending increases in these and other areas, nanofabrication itself is becoming a greater proportion of total energy consumption in the developed world. The costs of nanomanufacturing (defined very broadly) are becoming significant contributors

1) By "efficient use of energy" we imply also the efficient use of materials and water, with a minimal production of toxic waste.

Nanotechnology for the Energy Challenge. Edited by Javier Garcia-Martinez

ISBN: 978-3-527-32401-9

of the costs of running the society. It is important that nanoscience and nanotechnology grow in environmentally responsible ways–not only developing nanomaterials with low toxicity, but also minimizing the energy intensity of nanofabrication. Green techniques of nanofabrication and nanomanufacturing can make a significant contribution to energy sustainability.

In the past several years, many unconventional approaches to nanofabrication have emerged; many of these approaches share the characteristic–intentionally designed or not–that they are conservative with respect to energy. The emphasis on the fabrication of nanostructures is distinct from the important functions that nanotechnology is likely to fulfill in the energy economy: efficient microprocessors, heterogeneous catalysts for the production and use of fuels, systems for global carbon management [2], systems for solar energy harvesting (photovoltaics, lenses, mirrors), membranes for purification and separation (O_2, water, CH_4, CO_2, H_2 CO, small particles) [3], devices for communications (optical fiber and microwave technology), displays, systems for lighting, materials to reduce friction, lightweight nanocomposite materials for the transportation industry [4] and many others.

10.1.1 Motivation

All strategies for meeting future energy demands require both improved and alternative sources of power and improvements in the efficiency with which energy is used [5]. Any potential solution to the energy challenge may be severely constrained in its form by environmental concerns (especially global warming) and issues of national security (e.g., nuclear power). The scientific community is justifiably interested in technologies that have a large, long-term potential for the clean production of energy (e.g., photovoltaics, carbon sequestration). Progress in these areas has come in notoriously small increments, however. Correspondingly small increases in efficiencies of sufficiently large consumers of energy (e.g., water purification, indoor lighting) or small reductions in losses (e.g., due to electrical transmission or friction) would make an immediate impact on the conservation of energy.

Nanofabrication, in all of its forms, is already a significant consumer of energy and thus can be regarded as a target for strategies to reduce energy consumption [6]. We justify this assertion by briefly characterizing the energetic aspects of nanofabrication in the context of the semiconductor industry and in academic laboratories. We find high energetic costs associated with fabricating highly ordered nanostructures that resemble the forms–but not necessarily the functions–of microelectronic components. We do not focus on the fabrication of random bulk nanostructured materials in which the "nano" may be incidental (e.g., carbon fiber tennis racquets, cosmetics, simple porous membranes). We avoid these materials in part because it is difficult to estimate the energetic costs associated with manufacturing them and also because the criteria for materials that do or do not qualify as "nano" are unclear.

10.1.2 Energetic Costs of Nanofabrication

The manufacturing sector of the United States economy consumes 24% of all energy distributed. The computers and electronics industry accounts for 12% of the manufacturing sector, by economic value [7]. Electronic products are driven by the semiconductor industry, which is growing at 15% per year with concomitant increases in inputs of energy [8]. The reduction in size of semiconductor devices has come at a price of increased complexity of both the devices and the techniques used to manufacture them. Wilson *et al.* conducted a rigorous analysis of the inputs into the production of a 32 MB DRAM chip (weighing 2 g, measuring 1.24 cm^2) and concluded that 1.6 kg of chemicals were consumed during the process [9]. The value includes estimates of processing chemicals and fossil fuels consumed at every stage of device production, starting from quartz and including its conversion into silicon wafers, but excludes a large contribution from water combined with purified elemental gases, which have a substantial energy of production as well.

In semiconductor fabrication, the ratio of the weight of input materials to the weight of finished products (microchips) is several orders of magnitude higher than that for other manufactured goods. In fact, an average desktop computer consumes four times more energy in production than in use, over a three-year life cycle [10]. The total carbon footprint (in production plus use) of a desktop computer is 1.3× that of a refrigerator, even if the computer lasts 3 years and the refrigerator lasts 13 years [10]. While the production energy of a manufactured product should not be entangled with its value to society [8, 11], the minimization of the energy intensity of nanomanufacturing can be addressed most efficiently if divorced from its (difficult to estimate) societal costs and benefits. The notably high production energy associated with semiconductor manufacturing arises from the purity of the materials and chemicals, the high-precision processing tools, and the environmental control within the fabrication facility (fab).

Semiconductor fabs and academic cleanrooms are significant consumers of energy [12]. Hu *et al.* found an average power consumption value of 2 kW m^{-2} for fabs in Taiwan (this figure is typical for fabs in other countries as well) [13]. For comparison, a typical residential energy use is <10 W m^{-2} in the United States. A survey of an anonymous research-oriented nanofabrication facility, a modern class-100 cleanroom—where the class number refers to the number of particles >500 nm allowed per cubic foot of air—revealed a consumption rate of 3 kW m^{-2}. Figure 10.1 summarizes the power distribution within the cleanroom. Processing tools (evaporators, furnaces, etc.) consume two-thirds of the energy, while climate controls and air polishing (filtration) consume the balance. The proportions are reversed in industrial fabs, where tools consume one-third and climate controls consume two-thirds [13].

The energetic requirement *per unit output* of an academic cleanroom is significantly greater than that of an industrial fab, because the energy consumed *per area* by the two types of facilities is comparable. For example, the anonymous

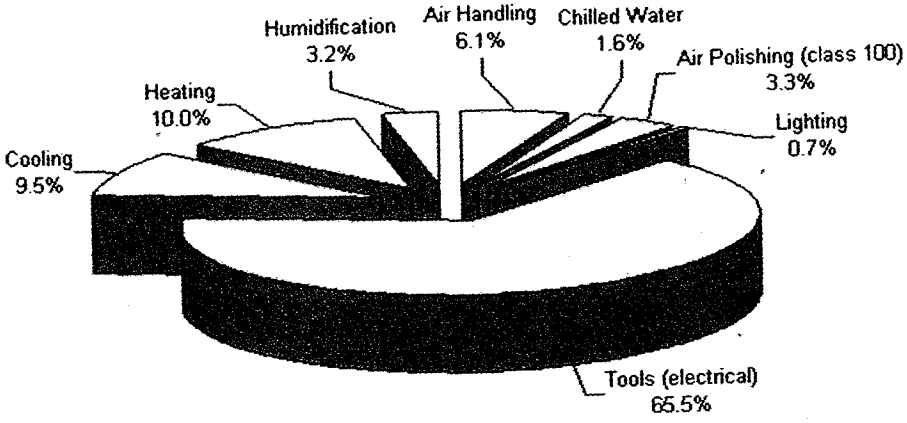

Figure 10.1 The power distribution of environmental controls, tools, and peripheral devices in a research-oriented, class-100 cleanroom. The cleanroom is 975 m^2 in area and in total consumes 3.0 MW. Electricity, including both lighting and processing tools, accounts for nearly two-thirds of the power.

cleanroom averages 100 users per day; liberally assuming that each user produces one finished wafer (or "experiment") per visit, the energy required for a single experiment is 2.7 GJ, which excludes the costs associated with chemicals and starting materials. This value is about 100 times greater than the analogous energy required by a fab to produce a 32 MB DRAM chip [9]. Conservation of energy usually is not a constraint when designing an experiment in a research setting, but economics usually is. The significant energetic costs of available techniques (which are almost always linked to economic costs) limit the extent to which fundamental studies of nanostructures may be carried out in academic laboratories.

We note that almost any process could be improved if performed under precise control over the environment and in the absence of dust. The extents to which processes and applications tolerate variations in climate and contamination can, however, vary greatly. A single defect might ruin an entire microprocessor, whereas a damaged feature of a nanostructured solar cell would be inconsequential. This chapter is not an attempt to label the semiconductor industry as inefficient or to dismiss high-precision instruments and cleanrooms as unnecessary. Such an interpretation would be wholly incorrect. In the event that a green approach produces a functionally equivalent structure to that of a conventional approach, the green approach should, however, be chosen. Economics–for better or worse–usually determine the choice in industry, unless sustainability is required by regulation.

10.1.3 Use of Tools

Processing tools are central to fabrication, and consume a significant percentage of the energy per experiment. Additional energy related to instruments goes into

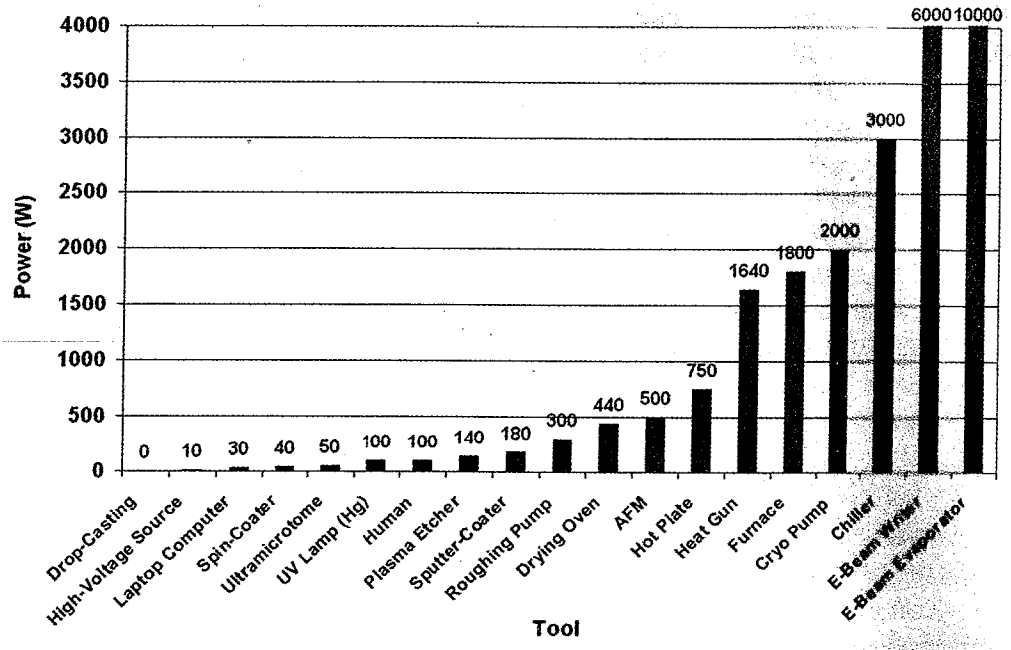

Figure 10.2 Power consumption values for common laboratory tools. All tools <1.8 kW were measured with a P3 "Kill A Watt" model P4400 commercial AC power meter except where otherwise noted. E-beam evaporator: maximum power of filament only. E-beam writer: Raith-150 maximum power. Chiller: recirculating water chiller maximum power. Cryo pump: CTI-Cryogenics compressor power rating. Furnace: Thermolyne model 48010 at 1200 °C max from manufacturer's specifications. Heat gun: Varitemp model VT 750-C at maximum setting. AFM: Veeco Nanoman manufacturer's maximum power rating. Hot plate: Cole-Parmer Instruments model 4658 with heating element on; add 19 W for maximum stirring speed. Drying oven: VWR Scientific Products 1300U. Roughing pump: Alcatel 2010 SD at base pressure. Sputter-Coater: Cressington sputter coater equipped with a Pfeiffer vacuum pump, model MVP 015-2, idling at base pressure 134 W, 180 W at 60 mA. Plasma etcher: SPI Plasma Prep II, idled at 47 W, vacuum pump not included. Ultramicrotome: Leica Ultracut UCT in normal operation with lights off, it consumes 32 W idle and 92 W with all lamps on. Spin-coater: Headway Research model PMW 32 at 3 krpm, does not include energy of house vacuum system. Laptop Computer: IBM ThinkPad T43p. High-voltage DC power supply: Spellman CZE 1000R at 10 kV.

a chilled-water system, which is required for heat management. Sophisticated tools can also have substantial large production energies, which are paid even if they are never used. Figure 10.2 shows typical values of power consumption for several key tools and peripheral devices discussed in this chapter. The power ratings were measured by us or taken from the manufacturer's specifications (see figure caption). Unsurprisingly, instruments that heat and cool are the largest consumers of energy, which include the filament of an e-beam evaporator, furnaces, heat guns, hot plates and chillers. Tools that produce a plasma or convert electrical energy into mechanical energy tend to consume less energy. Most instruments consume energy only when activated (e.g., heat gun), but some idle at their maximum power (e.g., drying oven) or a large fraction of it (e.g., because it is

wasteful and time-consuming to turn off and regenerate a cryogenic pump between uses of an e-beam evaporator).

Conventional tools of nanofabrication include electron-beam (e-beam) lithography (for creating lithographic masters) and photolithography (for replication). E-beam lithography is the dominant technology for the masterless creation of nanoscale features. It has the advantage of making arbitrary patterns at high resolution, but at the disadvantages of being serial, slow and energy intensive. Photolithography typically uses a photomask defined by e-beam lithography to transfer a pattern to a photoresist film. The technique is parallel and is the workhorse of replication for microelectronics. Lithography combines with processes such as physical vapor deposition (including sputter-coating, e-beam, thermal evaporation), reactive ion etching (RIE) and ion implantation to generate structures and to build complexity.

One of the strategies of unconventional approaches to nanofabrication is the adaptive re-use of analytical instruments for the purposes of fabrication. For example, instruments designed for analysis at the nanoscale can also be used as fabrication techniques, such as dip-pen nanolithography [14] (DPN, which uses an atomic force microscope) and nanoskiving [15] (which uses an ultramicrotome). Another strategy is to extract nanoscale information from unconventional sources. Thin films [16], shadows [17], edges [18], cross-sections [19], cracks [20] and lattice steps [21] can all be exploited for any nanoscale information they contain. The spontaneous organization of molecules into nanostructures (self-assembly) also has significant potential in nanofabrication [22]. The creative use of tools, the extraction of nanometric information from unconventional sources, and the discovery of new phenomena in self-assembly are thus central to this chapter.

10.1.4 Nontraditional Materials

The use of nontraditional materials is expected to reduce significantly the costs associated with nanofabrication. High-purity silicon wafers for microelectronics are produced in a sophisticated and energy-intensive process, which requires ~10 GJ kg^{-1} of electricity (~3000 kWh, ~2 t of CO_2) and has a yield of silicon of 9.5% from quartz, including all steps of manufacturing [9]. The formation of nanostructures from semiconductor nanocrystals [23], π-conjugated polymers and small molecules [24], materials derived from sol-gel precursors [25], and other nontraditional materials often cannot be accomplished with conventional techniques. The fabrication of devices based on these materials thus provides additional motivation for the development of new ideas in nanofabrication.

10.1.5 Scope

The concept of reducing the use of energy and raw materials is well established in the field of chemistry. A manifestation of this trend is in the impact factor of

the journal *Green Chemistry*, which has risen steadily in the decade since the journal's inception [26]. Some of the tenets of green chemistry are also applicable to green nanofabrication, including the substitution of "harsh" processes for "mild" ones (temperatures, pressures, etc.), the use of water [27] and supercritical CO_2 [6] as solvents and the exploitation of self-assembly wherever possible.

Previously, we reviewed several unconventional approaches for nanofabrication – embossing, molding, printing, scanning-probe lithography, edge lithography, self-assembly [1, 28]. Unconventional approaches to nanofabrication tend to be low-cost alternatives to e-beam and photolithography and are simple enough to be accessible to users in fields far removed from solid-state physics and electrical engineering, such as biology and chemistry. They were invented, in part, to expand the scope of applications of nanostructures; while the conservation of energy was incidental in the invention of these techniques, it is the focus of this review.

We consider green nanofabrication a subset of both green chemistry and unconventional nanofabrication. Green techniques share many (but not necessarily all) of several key characteristics. They tend to: (i) be parallel, rather than serial, (ii) produce little waste by being additive, rather than subtractive (i.e., they form structures by successively adding or assembling materials rather than etching or discarding large fractions of material), (iii) benefit marginally or not at all by the use of a cleanroom or another form of strict environmental control, (iv) have the fewest number of steps possible, (v) replace materials that are costly to mine and purify, such as high-quality silicon, with widely available or synthetic materials, (vi) use simple, low-energy instruments and (vii) have the potential for large-area (>cm^2) fabrication.

This chapter is organized in terms of general approaches for green nanofabrication. Each section describes the general strategy and then gives examples of relevant techniques. Potential applications are emphasized throughout, although we pay particular attention to techniques for emerging applications of nanostructured materials – rather than techniques that are only intended for integration into semiconductor fabrication. The summary of each section compares the technique with others that are capable of producing similar structures. Many approaches in the literature can be regarded as green, but we must restrict our attention, in the interest of space, to a relatively small number of them.

The unconventional approaches to nanofabrication discussed in this chapter occupy a range of developmental stages. For example, block copolymer lithography is already incorporated into commercial processes in semiconductor fabrication [29], while step-and-flash imprint lithography (SFIL) is regarded as a practical technology for its cost, whole-wafer printing capability and potential to surpass the limits of resolution of photolithography imposed by optical diffraction [30, 31] (currently 40 nm; prospectively 15–20 nm in commercial production). Other techniques, such as particle replication in nonwetting templates (PRINT) [32] and nanoskiving [15], have promising capabilities but are in their exploratory stages. Our selection of techniques is idiosyncratic and emphasizes techniques in which pattern transfer – from one material or dimension to another – is a key step. The techniques produce or have the potential to generate long-range, laterally ordered

or multicomponent nanomaterials, which are required for electronics, optics, photovoltaics, fuel cells, sensing and other applications.

10.2 Green Approaches to Nanofabrication

10.2.1 Molding and Embossing

Molding and embossing are perhaps the most successful strategies for unconventional nanofabrication [1]. The resolution of molding and embossing is limited only by the graininess of matter and thus has the potential of circumventing the theoretical limits of photolithography set by diffraction. These techniques are divided into two categories depending on whether the pattern transfer element (the mold or stamp) is hard or soft. Techniques that require a hard mold include nanoimprint lithography (NIL) [33–35] and step-and-flash imprint lithography (SFIL) [36, 37], while those that use a soft mold include replica molding (REM) [38, 39], solvent-assisted micromolding (SAMIM) [40] and particle replication and nonwetting templates (PRINT) [32]. A molding or embossing technique, *per se*, cannot generate nanoscale information; it relies on other patterning techniques, usually e-beam- or photolithography, to pattern a hard mold directly or to pattern a master for a soft mold. The extent to which these techniques can be used to conserve energy, therefore, depends on: (i) the techniques used to prepare the mold and (ii) the number of times the mold can be reused.

10.2.1.1 Hard Pattern Transfer Elements

Embossing using hard molds in various forms has been used commercially on the sub-micron scale for decades in the production of compact discs (CDs), DVDs, diffraction gratings and holograms [1]. The most common hard molds are made from quartz, silicon and metals. They are prepared by first patterning a resist film on the flat substrate by e-beam or photolithography and then modifying the exposed regions using reactive-ion etching, wet etching or electroplating. Quartz molds have the advantage of optical transparency, which enables registration with preexisting features on the substrate. The smallest lateral features transferred into quartz and silicon molds are 20 and 10 nm, using e-beam lithography [1].

Nanoimprint lithography is the use of a hard mold to emboss a polymer heated above its glass-transition temperature. This technique is an important element in the toolkit of nanofabrication, but has been reviewed extensively elsewhere [1]. SFIL is a variation of nanoimprint lithography [41]: it replaces the photomask in traditional photolithography with a quartz mold, which renders complex optical systems unnecessary. It is performed at ambient temperature, low applied pressures ($<1\,lb\,in^{-2}$; n.b., equivalent to <7 kPa) and avoids the baking and solvent processing steps of photolithography. An additional benefit is that the transparent mold facilitates alignment and registration. The accuracy of alignment in SFIL is

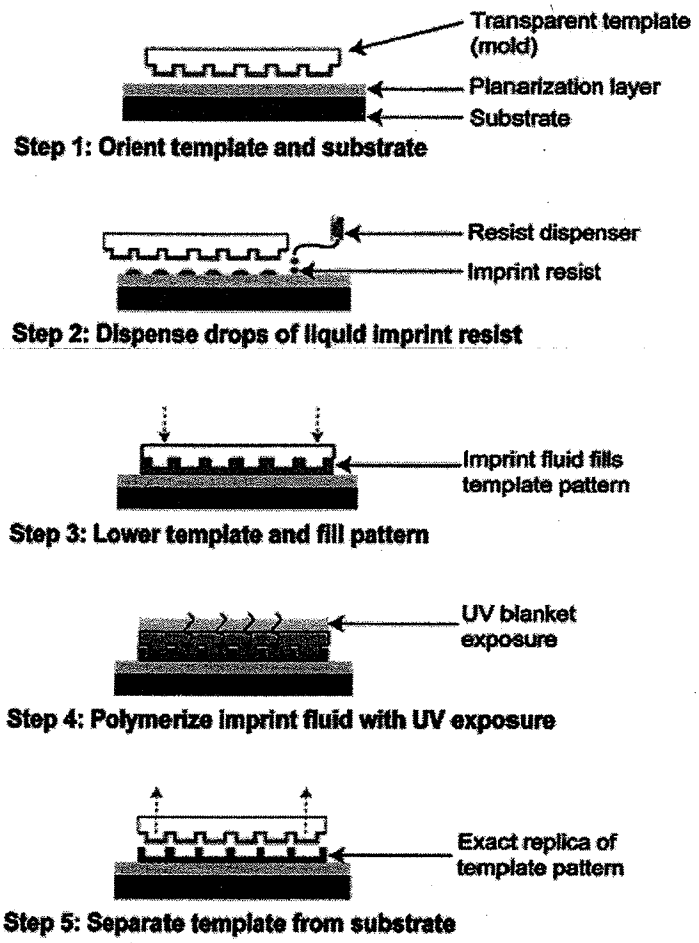

Figure 10.3 Schematic illustration of the SFIL process. A transparent mold (quartz) is pressed into a layer of imprint resist, a photocurable prepolymer. UV irradiation cures the imprint resist, after which the mold is removed. The resist contains a relief structure of the original mold, which can direct further modification (etching, evaporation, ion implantation, etc.) of the substrate. Reprinted with permission from [42]. Copyright 2008, American Chemical Society.

as high as ±10 nm (3σ) [36]. SFIL thus has potential for incorporation into microprocessor fabrication [30].

SFIL works by molding a photocurable prepolymer (imprint resist) with a quartz template against a flat substrate. The prepolymer is irradiated and crosslinked through the transparent mold. Release of the mold reveals the relief structure in the crosslinked polymer. A residual (scum) layer connects the molded features in the imprint resist to one another. A breakthrough etch removes the scum layer and completes the pattern transfer step. The unconnected features of imprint resist can then direct further elaboration of the substrate [30]. Figure 10.3 summarizes the process.

The use of hard molds can save energy in nanofabrication as long as the molds are reusable. Increasing the lifetime of a hard mold is a significant challenge and

an object of research for the adoption of molding techniques in industrial nanofabrication. Deposition of crosslinked polymer on the mold (fouling) can cause irreversible adhesion of the mold to the substrate. Treatment of the mold using fluorinated silanes lowers the surface energy of the mold and extends the lifetime, but fewer than 100 uses per mold is typical [1].

A new approach has been described in which the imprint resist material is crosslinked with a linear molecule containing a selectively cleavable functional group along its backbone [41, 42]. The most successful group used was an acetal, which is labile in acidic solution. A mold contaminated with this material could be cleaned by de-crosslinking the polymer adhered to the features of the mold with a simple acidic wash. Figure 10.4 shows the cross-section of a SiO_2 stamp filled with a reversibly crosslinked imprint resist (top) and a different stamp after dissolution of the resist (bottom). In this study, all traces of crosslinked imprint resist could be removed by a simple acidic wash. While a statistical analysis of the lifetime of molds using this technique was not reported, the development of imprint resists that can be washed from the molds is an important line of research in SFIL.

10.2.1.2 Soft Pattern Transfer Elements

Soft molds are prepared by casting a prepolymer against a photolithographically patterned master, in a collection of techniques known as soft lithography [43]. The most common material used for this purpose, by far, is poly(dimethylsiloxane) (PDMS). PDMS is an elastomer with several useful characteristics, including chemical inertness, durability, transparency above 280 nm and the ability to pattern curved substrates [43]. The polymer is available in several commercial formulations; our laboratory uses Dow Corning Sylgard 184.

In the process of replica molding (REM), a photolithographically patterned master structure templates a PDMS mold, which then molds another polymer. Individual PDMS molds have been used more than 20 times in the context of the replica molding process, although a practical maximum for the number of replications has not been established. PDMS can replicate features in a topographically patterned master down to the atomic scale (0.2 nm), as demonstrated by Xu and coworkers by casting the polymer against a crack in a Si wafer [20].

In solvent-assisted micromolding (SAMIM), a solvent softens or dissolves a polymer film. A PDMS stamp is placed in contact with the polymer. During evaporation of the solvent, the polymer film conforms to the features of the PDMS mold. SAMIM has been used to pattern lines with widths of 60 nm in a Novolac photoresist [40]. This process is also amenable to several other polymers, including polystyrene (PS) [40], poly(methylmethacrylate) (PMMA) [40] and cellulose acetate (CA) [40]. A related technique, micromolding in capillaries (MIMIC), has been used to fabricated conjugated polymer field-effect transistors [44]. Like SFIL, SAMIM leaves behind a scum layer in the patterned polymer film. Figure 10.5 summarizes the SAMIM process.

Nonlithographic master structures may also be used to template the formation of a mold. McGehee and coworkers used a nanoporous anodic aluminum oxide

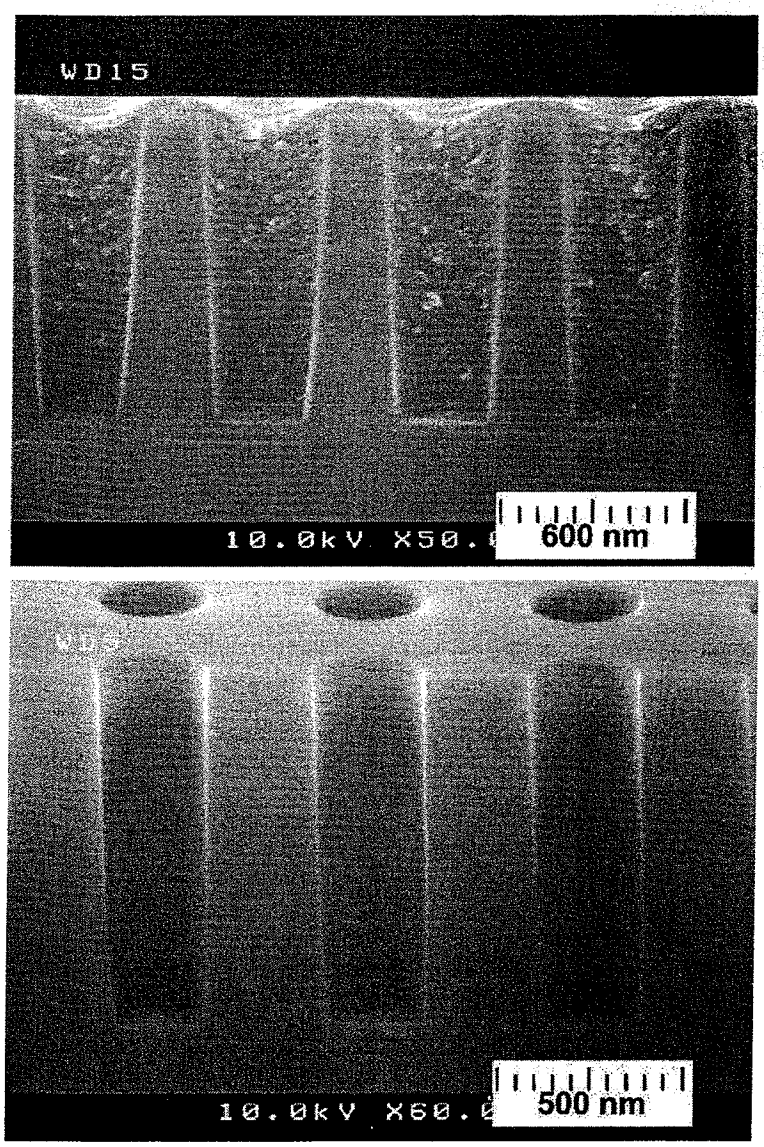

Figure 10.4 Scanning electron micrograph of a SiO_2 substrate patterned with pores with reversibly crosslinked imprint resist (top) and a different sample after de-crosslinking and dissolving the imprint resist (bottom). Reprinted with permission from [41]. Copyright 2007, American Chemical Society.

(AAO) template to direct the formation of a PMMA mold, which contained a relief structure of the template – nanopillars of 35–65 nm diameter with aspect ratios up to 3 [25]. This mold, in turn, was used to stamp a titania sol-gel precursor film, which was then calcined. In this way, the morphology of the nanostructured AAO template could be transferred to semiconducting metal oxide films. The choice of PMMA was necessary because of the high compression modulus (~2–3 GPa) compared to that of PDMS (~2 MPa), which was unable to keep the high-aspect-ratio features rigid. While both the AAO template and the PMMA mold

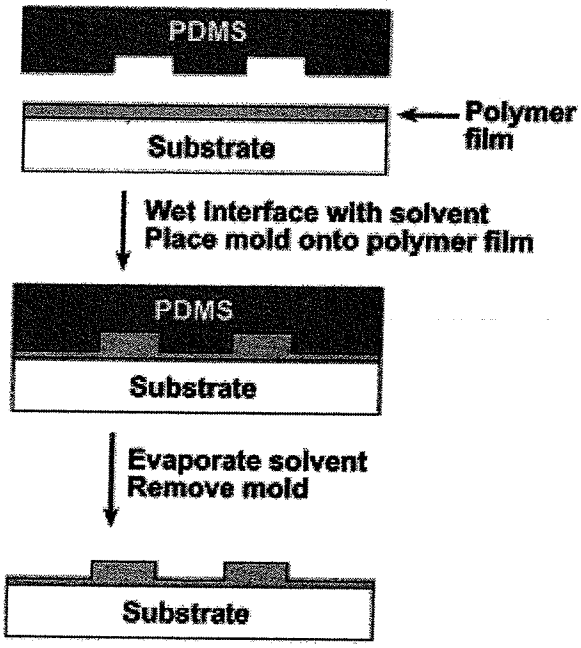

Figure 10.5 Schematic illustration of SAMIM. A PDMS mold is wet with solvent and placed in contact with a polymer film. After evaporation of the solvent, the mold is released. A relief pattern of features remains in the polymer film. Reprinted with permission from [1]. Copyright 2005, American Chemical Society.

are consumed by dissolution during the process, both materials are inexpensive and readily available. High-surface-area structures are believed to facilitate charge collection in excitonic solar cells (including polymer, small molecule, semiconductor nanocrystal-based devices) [45–47].

The ability to tailor the surface chemistry of molds is paramount to the success of molding techniques. SFIL, NIL, RM and SAMIM usually yield a residual layer (scum) between embossed features, which must be removed with a breakthrough etch step. The use of photocurable perfluoropolyether (PFPE)–a nonswellable, nonwettable elastomer (8–10 dynes cm^{-1}; n.b., 10 dynes = 10^{-4} N)–as both a mold and a flat template do not form a scum layer when embossing many types of materials. In a technique called *p*article *r*eplication *in* *n*onwetting *t*emplates (PRINT, Figure 10.6), DeSimone and coworkers showed that embossing films with PFPE templates produces discrete, unconnected particles, which can be easily detached from the substrate and harvested [32]. Examples of polymers molded into discrete nanoparticles include poly(ethylene glycol diacrylate), triacrylate resin, poly(lactic acid), poly(pyrrole) [32] and proteins [48]. Potential applications for these monodisperse nanoparticles include electronics and drug delivery [49].

The PRINT technique was recently extended to the preparation of discrete particles of inorganic oxides derived from sol-gel precursors [50]. First, a liquid sol was filled into the cavities of a mold. The mold was placed face-down on a substrate and held at an elevated temperature, at which the material underwent the sol-gel

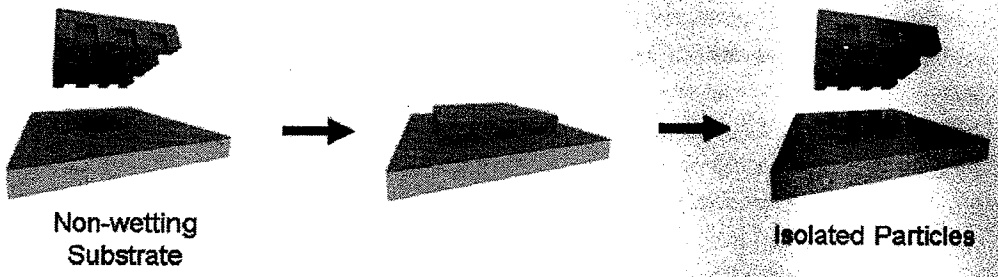

Figure 10.6 Schematic drawing of the PRINT process. A solvated precursor is compressed between a nonwetting substrate and a PFPE mold. The procedure produces isolated particles, which is a unique capability among soft lithographic techniques. Reprinted with permission from [32]. Copyright 2005, American Chemical Society.

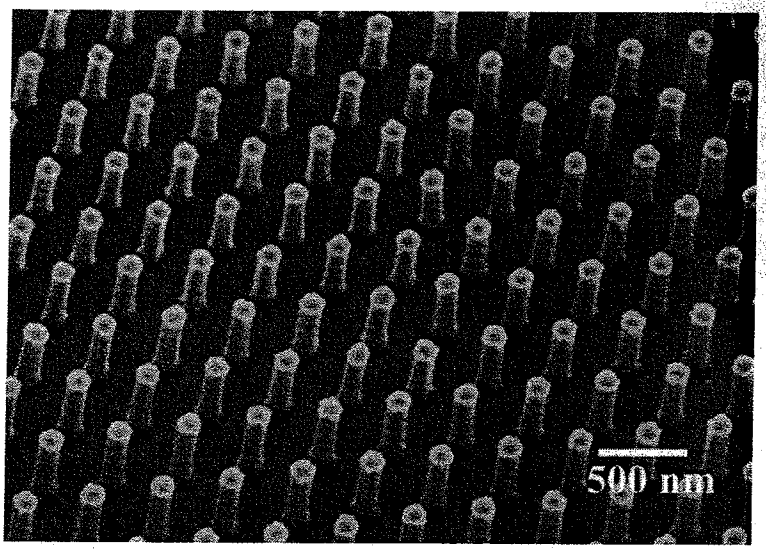

Figure 10.7 SEM image of discrete anatase TiO_2 nanopillars fabricated by PRINT. Reprinted with permission from [50]. Copyright 2008, Wiley-VCH Verlag GmbH & Co. KGaA.

transition. Removal of the mold revealed isolated oxide particles in their xerogel state. Calcination provided the crystalline phase. This strategy was able to produce either isolated features or embossed films of TiO_2, SnO_2, ZnO, ITO and $BaTiO_3$. Figure 10.7 is a SEM of isolated TiO_2 nanopillars, which could be useful, for example, as high-surface-area nanoelectrodes for excitonic solar cells. The sheer range of materials amenable to the PRINT technique makes it one of the most promising soft lithographic techniques for molding and embossing.

10.2.1.3 Outlook

The energetic costs of molding and embossing are tied to the fabrication and lifetime of the molds. The creation of arbitrary patterns with maximum resolution still requires the use of e-beam lithography and other conventional techniques;

nonlithographic patterns, such as porous block copolymer films or AAO membranes, avoid these limitations, but are only available in a limited number of patterns.

Once a mold is fabricated it can be reused several times, much in the way that a mask can be reused in photolithography, with the important difference that molds are subject to surface fouling and deterioration with repeated use (particularly hard molds). New materials, surface treatments and imprint resists are required to decrease the cost of molding and embossing. Soft molding techniques overcome some of the difficulties associated with surface fouling of the mold, because the low surface energy and mechanical flexibility facilitates detaching the mold from the substrate. The native surface energy of PDMS is 21.6 dynes cm^{-1}, which may be lowered by passivation with a fluorosilane to a the value to ~12 dynes cm^{-1}, which is similar to the value for poly(tetrafluoroethylene) (Teflon) [1]. Each photolithographic master patterned with SU-8 negative photoresist on a Si wafer and fluorosilanized is capable of producing >50 PDMS stamps. The lifetime of PDMS molds has not been established rigorously, but in our experience the features do not deteriorate if used at room temperature over a period of several months for >50 uses each. The number of end uses that can be derived from one step of photolithography (one trip to the cleanroom) is therefore >2500. The PRINT technology is a particularly exciting technology in the toolbox of soft lithography, as it has the advantage of making discrete nanoparticles in addition to two-dimensional surface patterns.

10.2.2 Printing

Nanofabrication by printing is the transfer of material from a topographically patterned stamp or movable tip to a surface. In a general sense, the advantages of printing are its potentially high throughput and the fact that it accommodates many types of materials. In terms of the conservation of energy, printing is green because it is additive: material is deposited only where it is required. (Conventional lithography is subtractive: large amounts of photoresist and other materials are usually discarded during spin-coating, development and any lift-off processes.) This section describes recent developments in two different types of printing: (i) microcontact printing (μCP) [43], which is a soft-lithographic technique that uses a stamp and (ii) dip-pen nanolithography (DPN) [14], which is a direct-write technique that uses an AFM tip.

10.2.2.1 Microcontact Printing

The most common incarnation of printing strategy is microcontact printing (μCP), which can be used to pattern alkane thiolates, silanes, biomolecules, colloidal particles, and polymers on metal and semiconductor surfaces [43]. Microcontact printing has been reviewed elsewhere [43], but we note that its key element is the generation of a topographically patterned stamp, usually PDMS, from a master that is typically patterned by photolithography. Printing self-assembled monolay-

ers (SAMs) of alkane thiolates on metal surfaces is the most prevalent form of μCP. SAMs can alter the wetting properties of surfaces and template the formation of secondary structures of another material. SAMs can also be used as resists for a variety of wet-etching processes. The lateral resolution of μCP can be <100 nm; it depends on the properties of the stamp and the extent to which the "ink" diffuses across the substrate. The smallest features transferred into a metal film by selective etching were 35 nm trenches separated by 350 nm [51].

A series of strategies of μCP can also be used to pattern features from a stamp that are smaller than those on the original master [52]. For example, mechanical deformation of the PDMS stamp can cause the features to converge; the lateral spreading of the contact area with the surface decreases the spacing between features. A single stamp can thus generate submicron linewidths by compression using a stamp patterned with lower resolution. Swelling the stamp with a solvent can be used to achieve a similar effect [52]. An extension of μCP, electrical-μCP, uses a PDMS stamp coated with a metallic film to print charge into a film of a dielectric polymer, PMMA [53]. Patterned charge can potentially be used as a high-density storage system for digital information. The resolution obtained in this study was 100 nm, but the theoretical limit has yet to be established. The energetic costs associated with μCP are similar to those of any soft-lithographic technique and depend largely on the number of prints a single stamp can make. Our laboratory has found that stamps may be reused over the course of months without noticeable deterioration in quality.

10.2.2.2 Dip-Pen Nanolithography

The Mirkin laboratory has developed a direct-write process using an AFM tip known as dip-pen nanolithography (DPN) [14, 54]. In DPN, the AFM tip is inked in a solution placed into contact with a surface. Direct transfer of the ink to the surface can create nanoscale patterns in arbitrary geometries. DPN accommodates a range of inks, including alkane thiols, proteins, conjugated polymers, DNA, sol-gel precursors, metal salts and monomers for polymerization [14]. Like μCP, DPN is an additive technique–material is deposited only where it is required, so it avoids blanket exposure steps to chemicals and other processes. Figure 10.8 shows the way in which an AFM tip deposits material on a substrate: a water meniscus forms between the AFM tip and the substrate. The meniscus serves as a carrier for molecular transport. Like μCP, the first demonstration of DPN used alkane thiolate SAMs on Au [55]. An additional useful characteristic of DPN is that multiple inks can be deposited on the same substrate[56].

The use of a single AFM tip only allows the serial reproduction of patterns. Recently, however, massively parallel DPN was demonstrated, in which 55 000 AFM tips were connected in a microfabricated, two-dimensional array. This array was able to produce copies of a dot matrix map of Au features over a $1 \times 1\,cm^2$ area (Figure 10.9). The ability to produce arbitrary patterns should have applications in nanoscale bioassays and other areas [54].

Parallel DPN is a maskless technique that, in principle, combines the resolution of a mastering technique [58] like e-beam lithography with the throughput of

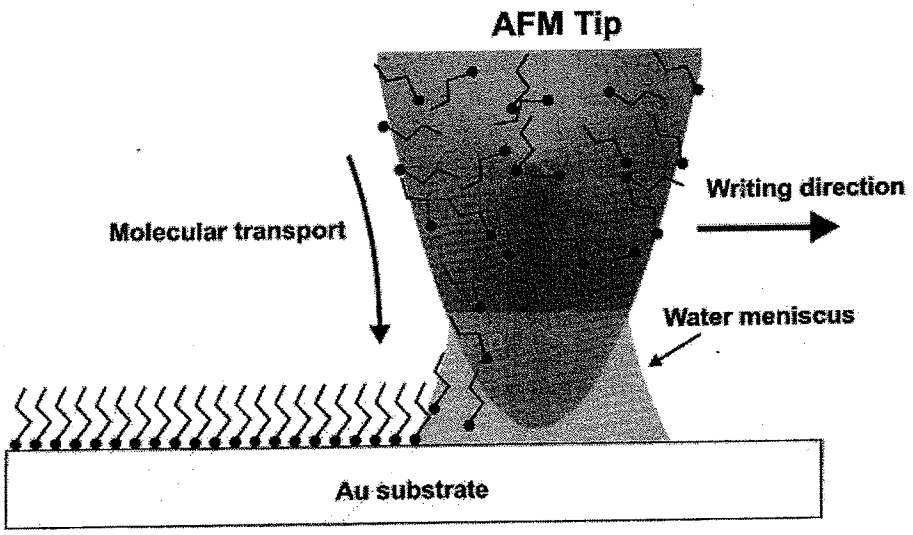

Figure 10.8 Schematic illustration of the DPN process. The AFM tip is "inked" with small molecules, which transfer to the surface of a solid substrate. Reprinted with permission from [55]. Copyright 1999, American Association for the Advancement of Science.

photolithography. It can serve simultaneously as a mastering step or a replication step. In the massively parallel process, each tip is passive and thus the whole array generates multiple copies of the same structure. There is no reason why the technique cannot be used to translate each tip independently, but this capability represents a significant challenge in engineering. As it stands, the DPN process is slow, but it is a promising new technology with unique capabilities. As a technique capable of generating masters, it may combine well with techniques requiring soft, patterned stamps.

10.2.2.3 Outlook

Nanofabrication by printing is now ubiquitous in research laboratories, and both μCP and DPN have significant potential for manufacturing due to their parallel capabilities. The additive nature of printing attenuates the production of chemical waste, which is produced in photoresist processing steps used in photolithography. The energy associated with the μCP process is in its use of conventional photolithographic mastering techniques, while the printing step itself can be done manually or with simple tools. DPN uses an AFM, a low-wattage instrument. There is evidence, however, that the transport of ink in the DPN process is a function of humidity and temperature of the ambient air [59]. Some control over the environment is necessary for the reproducibility of DPN.

10.2.3 Edge Lithography by Nanoskiving

Conventional lithography and thin film deposition are typically regarded as two-dimensional techniques. In many cases, the edges of structures (including the

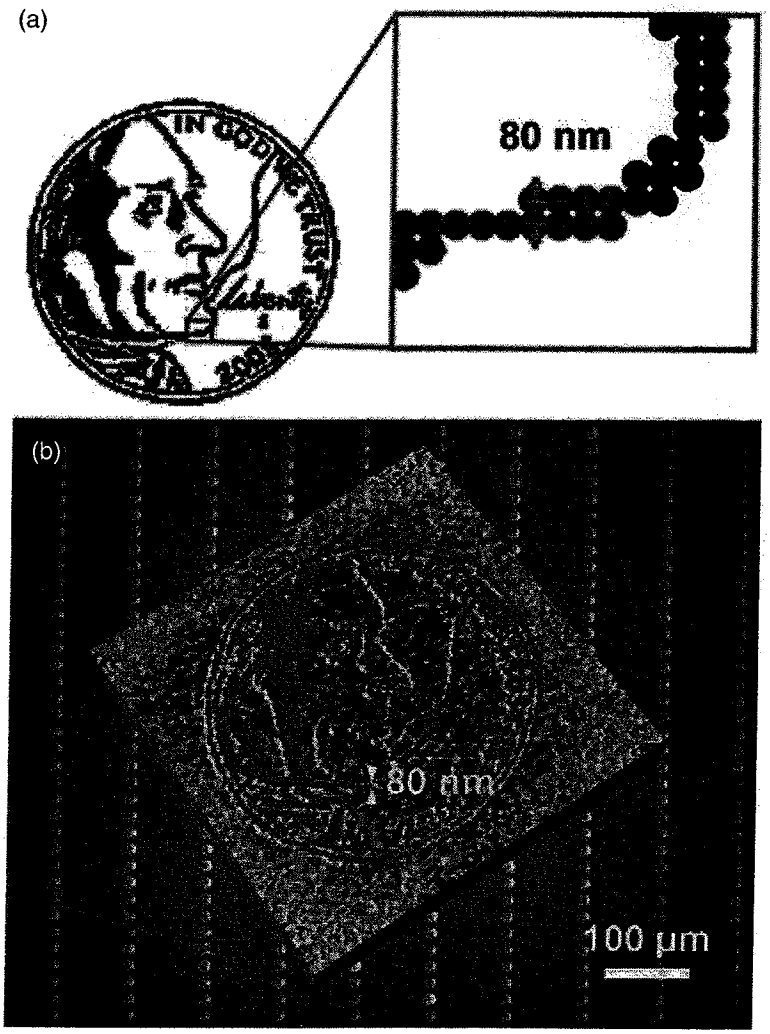

Figure 10.9 (a) An array of dots depicting the front face of a United States five-cent coin. (b) This image was reproduced in an array using the parallel array of AFM tips. Reprinted with permission from [57]. Copyright 2007, Wiley-VCH Verlag GmbH & Co. KGaA.

sidewalls of photolithographic features, heights of thin films and step edges of crystalline lattices) contain nanoscale information. Edge lithographic techniques extract such information in two general ways: (i) pattern transfer directed by the edge of a feature and (ii) conversion of a feature that is thin in the vertical dimension to a feature that is thin in the lateral dimension [1]. Since our initial reviews of unconventional techniques of nanofabrication [1, 28], our laboratory has expanded significantly the types of structures accessible by the technique of nanoskiving–fabrication by sectioning with an ultramicrotome–which falls under (ii) [15]. We have applied nanoskiving to generate nanostructures and heterostructures of a range of organic and inorganic materials. Applications of devices include frequency-selective surfaces (FSS) [60], single-crystalline plasmon resonators [61], chemical sensors [19] and organic photovoltaics (OPVs) [62]. The technique is

operationally simple, can access structures with lateral dimensions as small as 10 nm and can be completely nonphotolithographic: it requires only an ultramicrotome (which is accessible in almost any research setting) and a method for the deposition of thin films or chemically synthesized crystals. It is inherently conservative with respect to energy (particularly in concert with spin-coating) and raw materials, and a cleanroom is not required.

10.2.3.1 The Ultramicrotome

The ultramicrotome is a mechanical cutting tool that was originally developed for thin sectioning of biological specimens for electron microscopy. The instrument is low-energy and is capable of producing sections of 30-nm thickness with routine use. An ultramicrotome consists of a sample arm, a diamond knife attached to a water-filled trough, a movable stage/knife holder and a stereomicroscope (Figure 10.10). The steps of the procedure are: (i) embedding the master structure in a hard polymer matrix (Young's modulus >1500 MPa, typically epoxies or PMMA) to make the "block", (ii) trimming and aligning the block, (iii) sectioning the block into thin slabs and (iv) collecting the slabs, which slide from the edge of the knife to the surface of the water trough. The surface tension of the water prevents compression of the slabs, which tend to self-assemble into ribbons while floating on the surface of the water. After the slabs are collected, optional processing steps include wet or dry etching. The rest of this section illustrates examples of materials and structures that are amenable to nanoskiving to form functional devices.

10.2.3.2 Nanowires with Controlled Dimensions

The simplest application of nanoskiving is the sectioning of strips of metal to form nanowires with precise control of every dimension. Figure 10.11 illustrates the procedure. A silicon wafer is patterned with Au stripes (micron width), which are transferred to the surface of an epoxy substrate. The Au stripes are embedded in epoxy and sectioned with the ultramicrotome, which yields nanowires. These nanowires displayed clear, size-dependent plasmon resonances [63].

10.2.3.3 Open- and Closed-Loop Structures

Sectioning parallel to the surface of a topographically patterned metal film can generate arrays of open- or closed-loop structures. Figure 10.12 illustrates this variation of the procedure. A topographically patterned epoxy substrate, with posts patterned by replica molding, is coated on one or more sides of each post with a metal film, using shadow evaporation. Embedding these posts in additional epoxy and then sectioning it parallel to the plane of the topography generates arrays of open-loop structures. Closed-loop structures can be generated using a single step of metal deposition by using sputtering (a noncollimated source) to coat the sides of the posts uniformily. A grating with micron-width trenches is used as the master [64]. These metallic structures behave as frequency-selective surfaces [60] and can also serve as resists for further elaboration of the substrate [65].

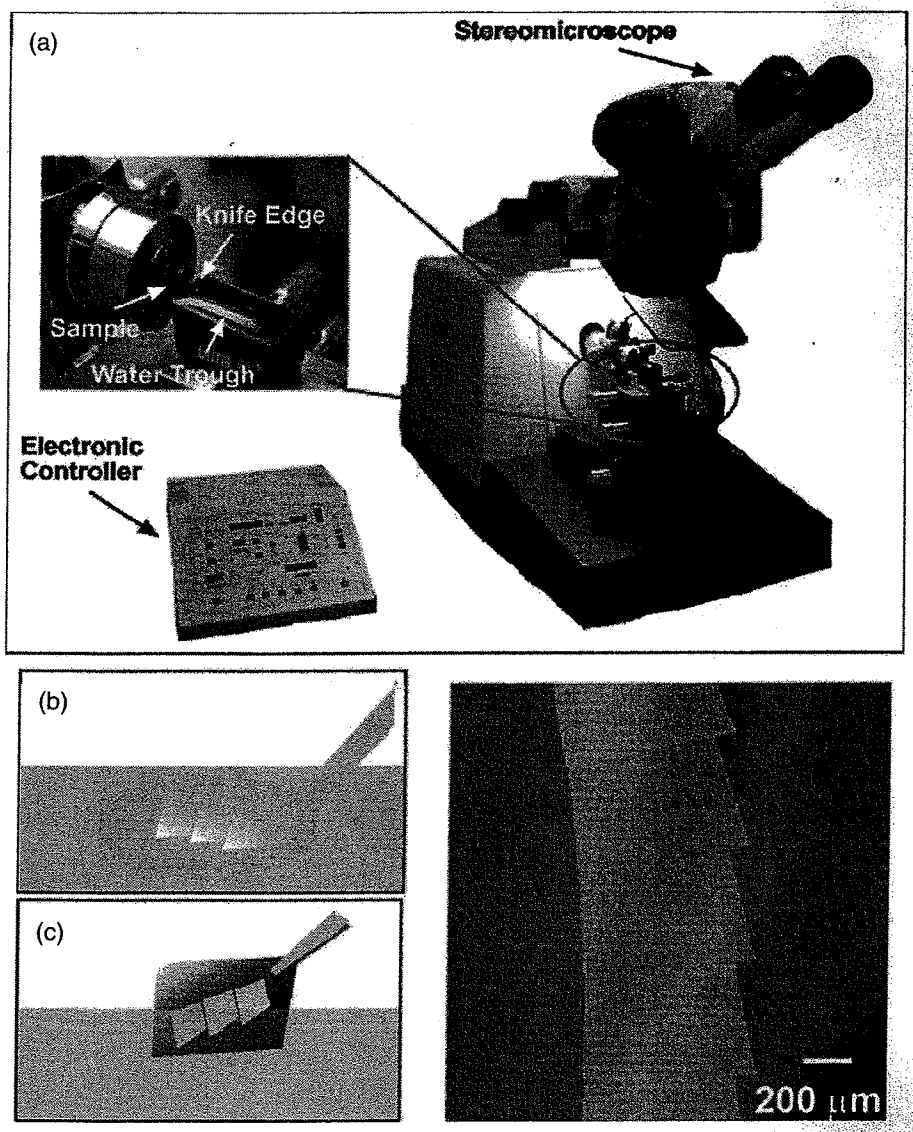

Figure 10.10 (a) Photograph of the model of ultramicrotome (Leica Ultracut UCT) used by our laboratory and close-up of the diamond knife and water trough. (b, c) Schematic illustration of collection of epoxy slabs with the use of a metal loop, which supports the slabs in a film of water, or by direct-capture with a substrate (a piece of a silicon wafer is depicted in 8F). (d) Micrograph of self-assembled epoxy slabs on the surface of water. Reprinted with permission from [15]. Copyright 2007, American Chemical Society.

10.2.3.4 Linear Arrays of Single-Crystalline Nanowires

Physical vapor deposition typically produces thin films that are polycrystalline. Sectioning these films, in turn, yields polycrystalline nanostructures, which are unsuitable for many applications. Chemically synthesized Ag nanowires have been shown to behave as low-loss plasmon resonators, with potential for use as waveguides in photonic integrated circuits and as biological sensors [66]. Silver

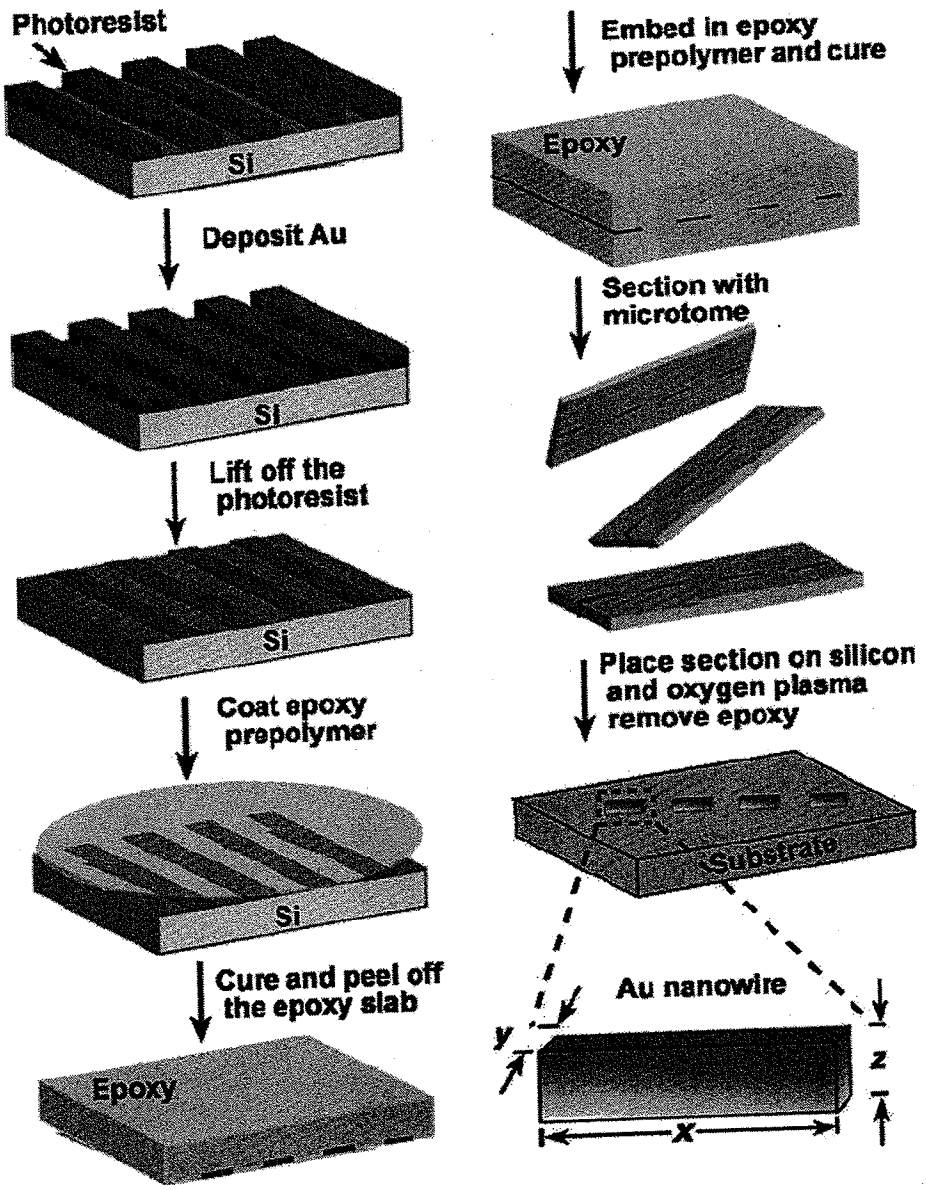

Figure 10.11 Schematic of the procedure used to fabricate Au nanowires. Reprinted with permission from [63]. Copyright 2006, Wiley-VCH Verlag GmbH & Co. KGaA.

structures, however, have limited potential for real applications because they are unstable due to oxidation under ambient conditions, oriented randomly on a substrate and polydisperse. Our laboratory used nanoskiving to fabricate single-crystalline nanowires of Au by sectioning chemically synthesized Au microplates [67]. The Au nanowires produced by nanoskiving also behave as plasmon resonators, but have the characteristics that they are stable to the atmosphere, oriented co-linearly within an epoxy slab, and reproducible from slab to slab. Figure 10.13 shows five quasi copies of a Au nanowire that were derived from a single microplate. The ability to produce monodisperse nanowires of this type has not been demonstrated using chemical synthesis alone.

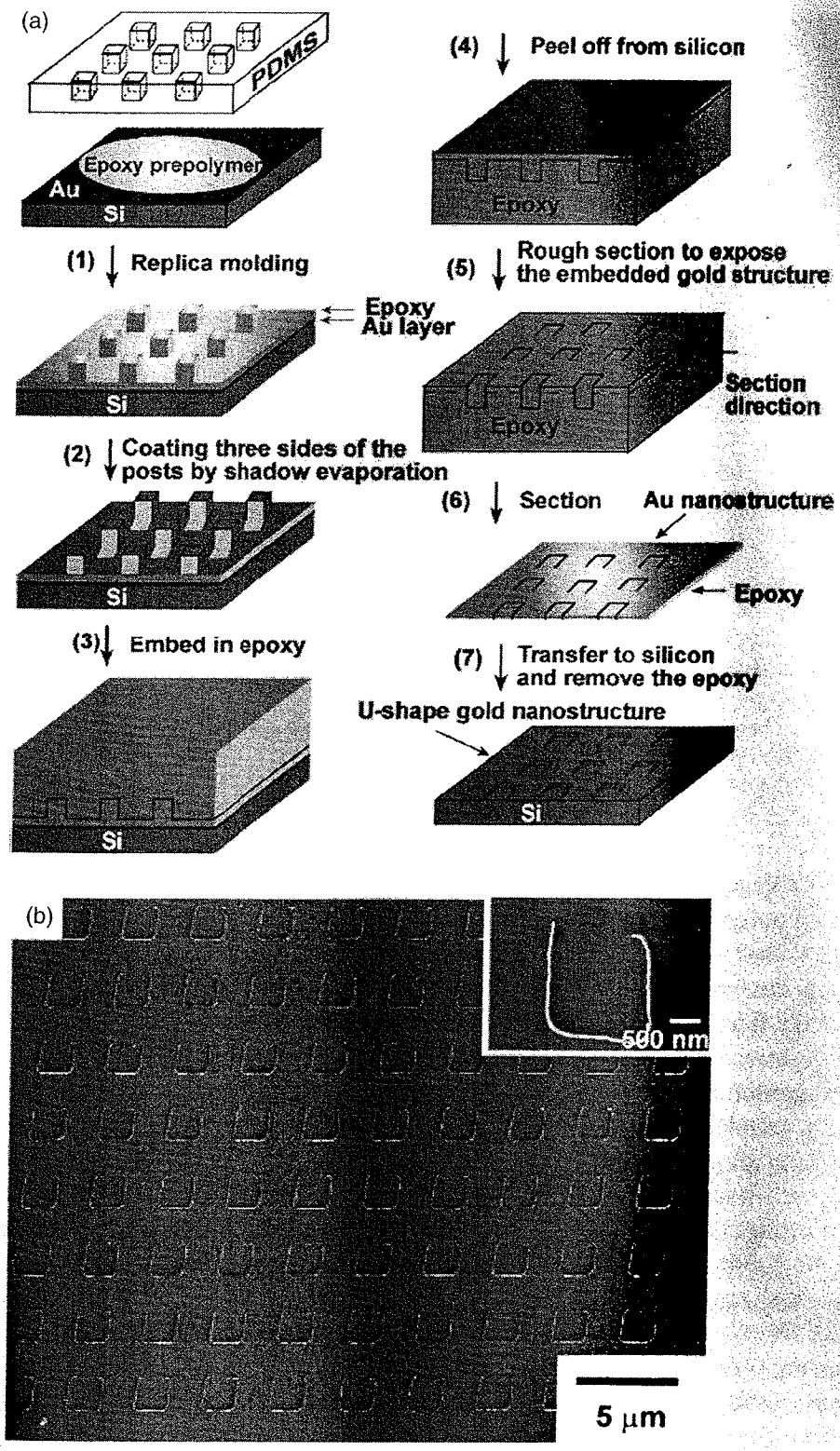

Figure 10.12 (a) Schematic illustration of the procedure used to generate complex metallic nanostructures from sectioning a topographically patterned surface (containing posts). (b) SEM images of structures obtained by sectioning parallel to the surface. Arrays of these structures serve as frequency-selective surfaces. Reprinted with permission from [15]. Copyright 2007, American Chemical Society.

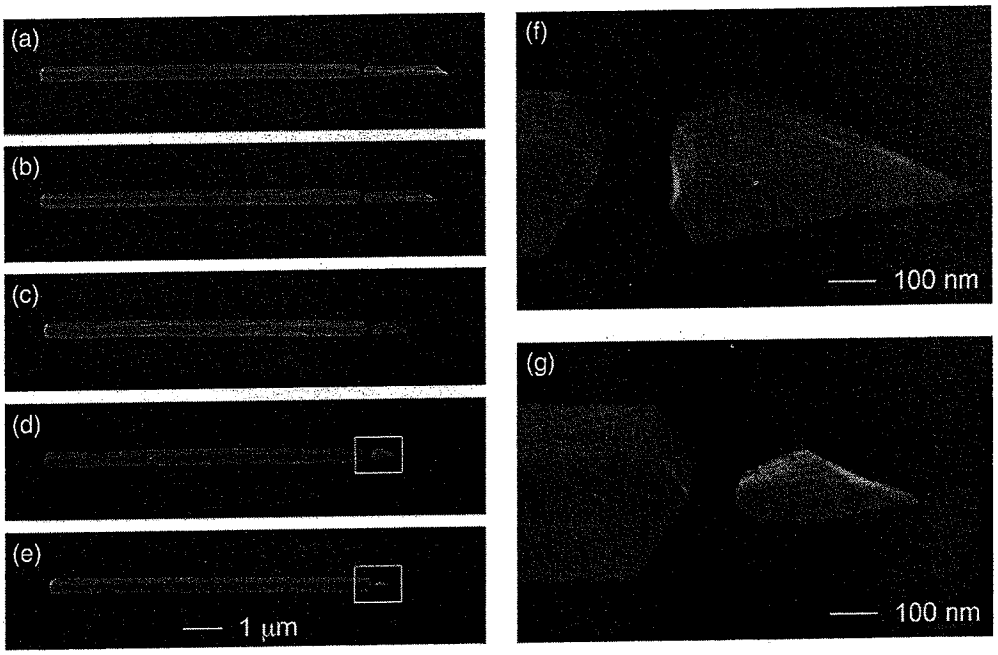

Figure 10.13 (a–e) Five quasi copies of a Au nanowire that were cut consecutively from a single hexagonal microplate. There is a section missing between (b) and (c). The structures on the right of (a–e) are nanowires derived from a smaller, triangular microplate (close-up shown in f, g). Reprinted with permission from [61]. Copyright 2008, American Chemical Society.

10.2.3.5 Conjugated Polymer Nanowires

Conjugated polymers possess many of the useful properties of crystalline semiconductors: electroluminescence [68], photovoltaic response [69] and modulation of conductivity by gate voltage [70] or by doping [71]. Polymers tend to be more mechanically flexible and less expensive to produce and process than crystalline semiconductors. As a result of this potential utility, there are many strategies for the fabrication and patterning of functional conjugated polymer structures [24]. One of the simplest (but most useful) structures is the nanowire [72, 73].

Potential applications of conjugated polymer nanowires include: chemical and biological sensors, field-effect transistors [74], tools for studying one-dimensional charge transport [75], actuators [76] and interconnects [77]. Nanowires composed of conjugated polymers are well-suited for sensing because they have a high ratio of surface area to volume, which permits rapid diffusion of an analyte to and from a wire [78, 79]. Electrical response and recovery rates are thus higher for nanowires than they are for thin films or fibrous networks. Electrochemical biosensors based on polymer nanowires have the potential for label-free detection of biological analytes. Incorporation of molecular recognition elements into conjugated polymers is relatively straightforward by synthesis, while analogous modifications of carbon nanotubes and inorganic nanowires require surface reaction(s) carried out postfabrication [80].

There is not yet a truly general technique for the fabrication of conjugated polymer nanowires, despite interest in the structures. In principle, any film-forming material can be formed into wires by nanoskiving, although the extent to which materials are damaged by the process depends on many properties. Many conjugated polymers are processible from solution and form stable films. We found that nanoskiving easily accommodates conjugated polymers. Figure 10.14 summarizes our strategy for the formation of two conjugated polymers with different physical and electronic properties, poly(2-methoxy-5-(2′-ethylhexyloxy)-1,4-phenylenevinylene) (MEH-PPV) and poly(benzimidazobenzophenanthroline ladder) (BBL).

The polymers can be identified in the SEM by etching. Figure 10.15a shows the transition between the composite MEH-PPV/BBL film and the free MEH-PPV nanowires. We obtained the image by covering a portion of the epoxy section with a conformal slab of poly(dimethylsiloxane) (PDMS) and treating the uncovered portion with a drop of MSA (as shown schematically on the left-hand side of Figure 10.15a) for ~5 s. We rinsed the MSA off the substrate with ethanol and removed the slab of PDMS. Figure 10.15b shows the transition between the intact composite film (right-hand side) and the free BBL nanowires after dry etching of the MEH-PPV and epoxy matrix (left-hand side).

When exposed to vapor from an I_2 crystal, the conductivity of the MEH-PPV nanowires increased by several orders of magnitude. Upon removal of the crystal, the conductivity rapidly decreased by the evaporative loss of I_2, which was concomitant with a decrease in free charge carriers. These results suggest that conjugated polymers formed by nanoskiving could function as high-surface-area sensors.

10.2.3.6 Nanostructured Polymer Heterojunctions

Given the fact that nanoskiving easily accommodates conjugated polymers, we sought to extend the technique to a different type of nanostructured architecture—the ordered bulk heterojunction for organic photovoltaics (OPVs). OPV devices are promising low-cost alternatives to solar cells based on crystalline semiconductors for the efficient production of electrical energy. Devices based on conjugated polymers, in particular, are ideally suited for coverage of many surfaces because they are processible from solution and mechanically flexible. One of the primary disadvantages of conjugated polymers (along with small molecules and semiconductor nanocrystals) is that they require a large amount of interfacial area between electron donating ("p-type") and electron accepting ("n-type") phases in order to separate photoexcited states (excitons) into free charge carriers (by photoinduced charge transfer). Once created, the electrons (e^-) drift toward a reflective, low-work-function electrode (LWFE), and the holes (h^+) drift toward a transparent, high-work-function electrode (HWFE). Additionally, the distance an exciton can travel before it decays (the exciton diffusion length, or L_D) is about ten times shorter than the thickness of material required for efficient absorption of photons (100–200 nm). The architecture that satisfies the requirements of both L_D and the thickness for optimal absorption of light is known as the ordered bulk heterojunc-

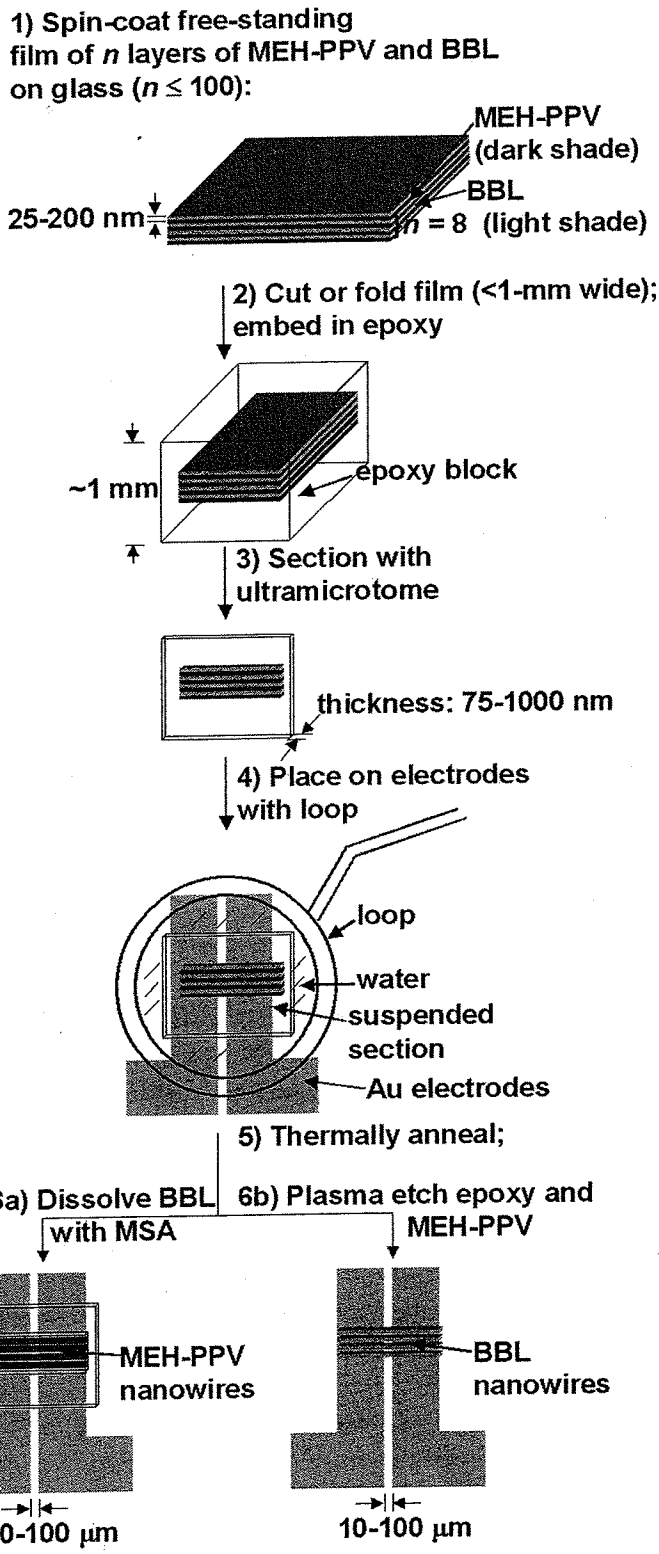
1) Spin-coat free-standing
film of n layers of MEH-PPV and BBL
on glass (n ≤ 100):
MEH-PPV
(dark shade)
BBL
n = 8 (light shade)
25-200 nm
2) Cut or fold film (<1-mm wide);
embed in epoxy
~1 mm
epoxy block
3) Section with
ultramicrotome
thickness: 75-1000 nm
4) Place on electrodes
with loop
loop
water
suspended
section
Au electrodes
5) Thermally anneal;
6a) Dissolve BBL
with MSA
6b) Plasma etch epoxy and
MEH-PPV
MEH-PPV
nanowires
BBL
nanowires
10-100 μm
10-100 μm

Figure 10.14 Summary of the procedure used for fabrication of multiple nanowires of MEH-PPV or BBL. We started by spin-coating a composite film of MEH-PPV alternating with BBL (step 1). Next, we cut the film into strips and embedded it in epoxy resin (the "block", step 2). We sectioned the block with an ultramicrotome (step 3), which yielded slices of the conjugated polymer film, framed by epoxy. Using a metal loop, we transferred manually the sections from the water boat of the ultramicrotome to photolithographically patterned Au electrodes on a SiO_2 substrate (step 4). Thermal annealing (step 5) improved adhesion between the thin sections and the electrodes. Selective dissolution of BBL with methanesulfonic acid (MSA; step 6a) gave free MEH-PPV nanowires or selective etching of MEH-PPV and epoxy with oxygen plasma (step 6b) gave free MEH-PPV or BBL nanowires. Reprinted with permission from [19]. Copyright 2008, American Chemical Society.

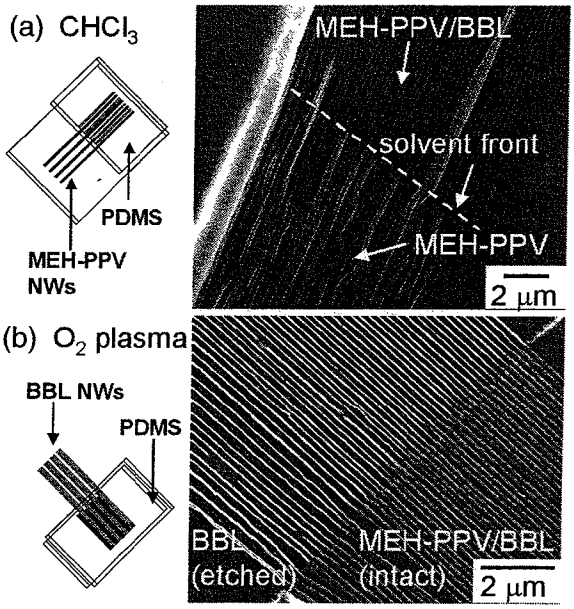

Figure 10.15 Scanning electron micrographs (SEM) showing the transition between the composite MEH-PPV/BBL film and free MEH-PPV nanowires (NWs). Reprinted with permission from [19]. Copyright 2008, American Chemical Society.

tion (Figure 10.16). It has a cross-section of p-type and n-type phases that is interdigitated on the length scale of L_D and is 100–200 nm thick.

We used nanoskiving to fabricate an ordered bulk heterojunction of two conjugated polymers in a three-step process: (i) spin-coating a composite film with 100 alternating layers of BBL (n-type) and MEH-PPV (p-type), (ii) rolling this multilayer film into a cylinder (a "jelly roll") and (iii) nanoskiving the jelly roll (Figure 10.17). The cross-section of a slab of the jelly roll has an interdigitated arrangement of the two polymers. The thickness of the slab is determined by the ultramicrotome and the spacing between the two materials is determined by spin-coating. Figure 10.18 shows a top-down image of a jelly roll slab embedded in an epoxy membrane, as well as a cross-section, which shows the interdigitated arrangement of MEH-PPV and BBL.

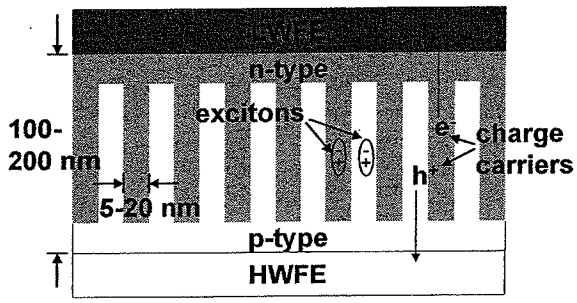

Figure 10.16 Schematic illustration of the ordered bulk heterojunction. Reprinted with permission from [62]. Copyright 2008, Wiley-VCH Verlag GmbH & Co. KGaA.

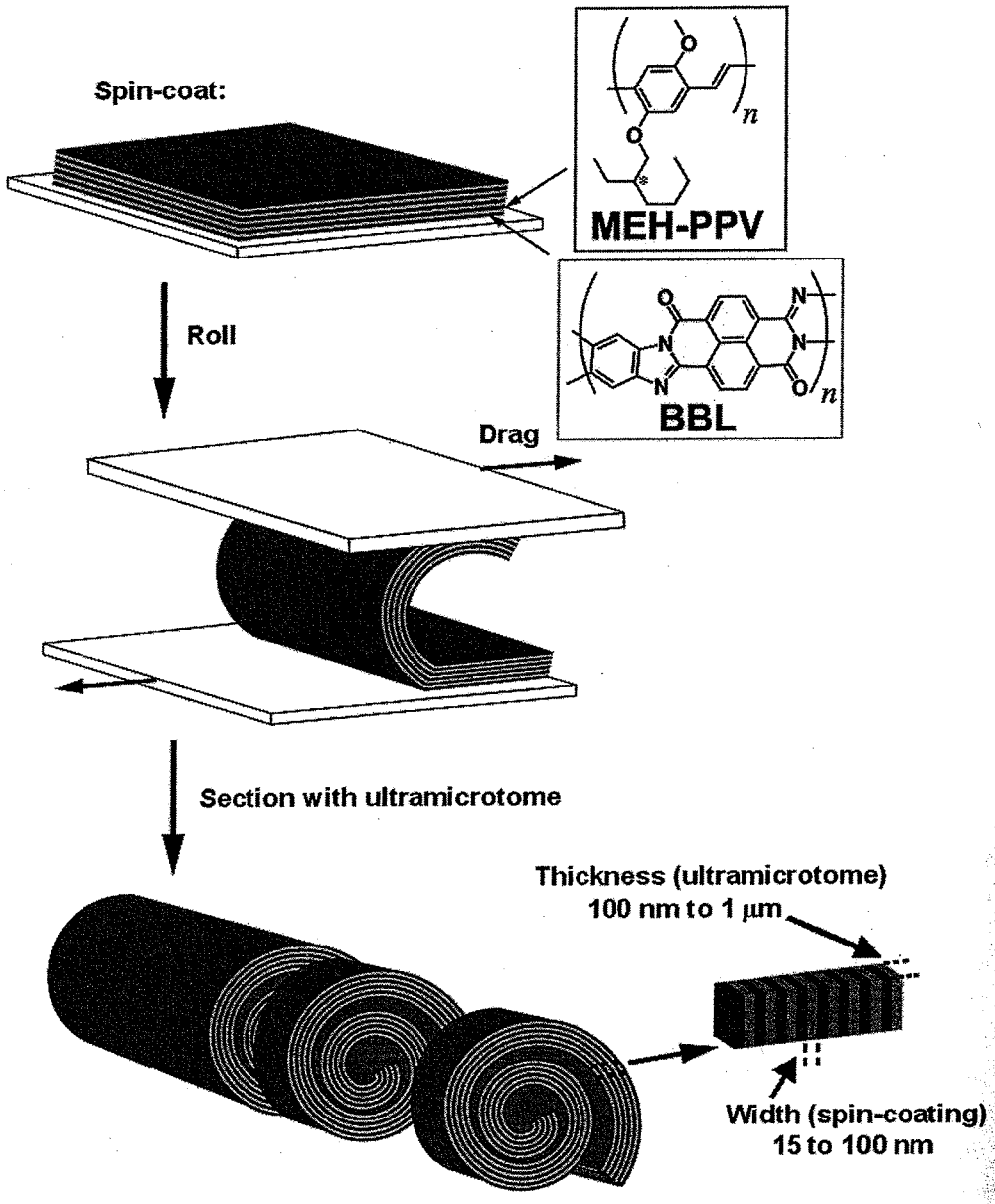

Figure 10.17 Schematic drawing of the procedure used to make nanostructured heterojunctions of MEH-PPV and BBL by nanoskiving a rolled, free-standing thin film (a jelly roll). Reprinted with permission from [62]. Copyright 2008, Wiley-VCH Verlag GmbH & Co. KGaA.

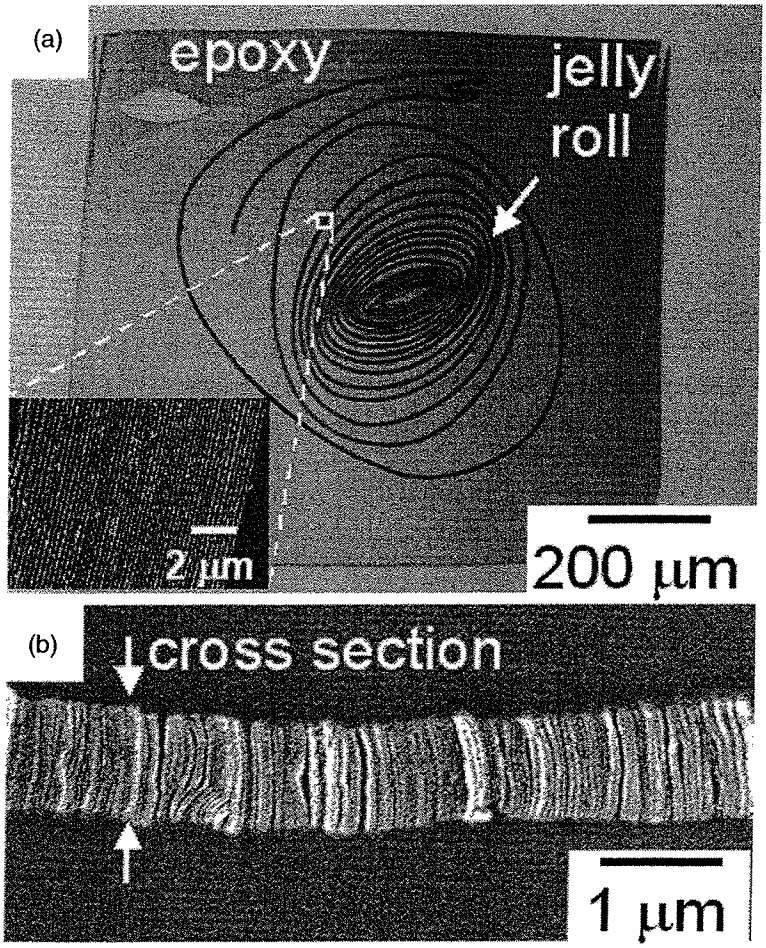

Figure 10.18 (a) Optical image of a slab of a jelly roll embedded in epoxy. The inset is an SEM close-up image of the exposed surface of the multilayer film of BBL (light gray stripes) and MEH-PPV (dark gray stripes). (b) Cross-sectional SEM of a slab of a jelly roll that shows the interdigitated structure of BBL alternating with MEH-PPV. Reprinted with permission from [62]. Copyright 2008, Wiley-VCH Verlag GmbH & Co. KGaA.

When placed in a junction between two electrodes with asymmetric work functions, the heterostructures exhibit a photovoltaic response under white light (although the efficiency of conversion of optical to electrical energy is low). Selective excitation of BBL with red light confirms that the photovoltaic effect is the result of photoinduced charge transfer between BBL and MEH-PPV. An initial experiment to determine the effect of n-type and p-type buffer layers between the jelly roll and the electrodes on the photovoltaic performance showed a marked increase in efficiency. Although the performance of the structure as a device is currently limited, we suggest that this approach to donor/acceptor heterojunctions could be useful in photophysical studies and might ultimately suggest new approaches to OPV devices.

10.2.3.7 Outlook

Nanoskiving is a simple and inexpensive technique in which nanoscale features are derived from the edges of thin films, not from two-dimensional photolithographic features. While some of the applications we described required the use of a photolithographically derived master, a cleanroom was not necessarily required for the micron-scale resolution reported here (only insofar as mask aligners are typically found in cleanrooms). In most applications of nanoskiving, the energetic costs associated with cleanrooms may be avoided entirely.

The structures produced by nanoskiving are embedded and stabilized in a thin epoxy slab, which is a macroscopic object that can be manipulated. These slabs may be placed on arbitrary surfaces, including curved substrates. If compatible with the nanostructured material contained in the slab, the epoxy can be removed by dry etching with an oxygen plasma.

Nanoskiving can access features with lateral widths as thin as 10 nm in several classes of film-forming materials. The technique shares this capability with only a few other methods, including scanning-beam and scanning-probe lithographies. These techniques, however, are not capable of producing large heights of features, which nanoskiving accomplishes easily. In this respect, nanoskiving has some analogy with nanoimprint lithography and deep reactive-ion etching, although the aspect ratios obtainable by nanoskiving can be significantly greater. Sectioning thin films into slabs with thickness ranging from 30 nm to 10 μm can produce structures with height-width aspect ratio of 10^3 (depending on the properties of the materials), which is not possible by any conventional technique.

Nanoskiving can function as a technique of both mastering and replication. As a mastering technique, it is somewhat like electron-beam or scanning-probe lithography; as a replication technique, it is analogous to photolithography or soft lithography. As potential manufacturing technique, nanoskiving is conservative with respect to raw materials because of the large number of quasi-copies that can be derived from a single block. For example, a 1-cm epoxy block in principle contains thousands of 100-nm sections. (Note that fewer sections may be produced when sectioning parallel to the surface of a topographically patterned film.)

The energetic costs of nanoskiving are low, particularly when sectioning spin-coated polymer films as the active material. An ultramicrotome consumes about 35 W when idling and 92 W during operation. Of these 92 W, 45 W are used by the lighting system, which may be turned off during operation of the instrument. A typical production energy value for epoxy, which is inexpensive, is 140 MJ kg^{-1} [9]. Diamond knives with a sharp wedge angle (35 °) give the best results, and, while they are expensive (US$1000–5000, depending on size and quality), may be re-sharpened after ~1 year of ordinary wear (at about half the cost of a new knife). Disposable glass knives are significantly less expensive, but are typically discarded after a single use.

As with any technique, nanoskiving has limitations. It is currently limited to structures with unconnected line segments, because the lateral features of the desired structure must be encoded in the cross-section of the block. Multilayer

patterning would, in principle, allow connectivity between features within a slab, but it would also erode the primary strength of nanoskiving—its simplicity. There is not yet a precise way to orient slabs on a substrate or to transfer them from one substrate to another. Some orientation is possible by hand using the perfect loop or direct transfer of slabs from the water trough to the substrate, but stacking sections to produce layered structures is difficult to accomplish with precise registration. The ultramicrotome also tends to compress samples somewhat along the axis perpendicular to the edge of the knife. This effect necessitates some flexibility in addressing the structures after sectioning and potentially limits the extent to which the slabs can be incorporated into precisely registered, multilayer structures.

10.2.4 Shadow Evaporation

Shadow evaporation is a method for forming nanoscale features by evaporating materials onto a substrate that is positioned at an oblique angle to the evaporation source, through a shadow mask, which determines the shape of projection of the beam of evaporated material onto the substrate [17]. Using different angles of evaporation for each material can form overlays of different materials.

10.2.4.1 Hollow Inorganic Tubes

Our group has used shadow evaporation to fabricate electrically continuous arrays of nanotubes of metals and indium-doped tin oxide (ITO) with controllable dimensions (height, outer diameter) [17]. We have shown these arrays to be useful as substrates for detecting small concentrations of organic molecules using surface-enhanced Raman spectroscopy. Potential applications exist for three-dimensional, nanostructured versions of devices, such as solar cells, light-emitting diodes (LEDs), electrochromics and batteries. For these devices, the nanostructured arrays provide: (i) a high ratio of surface area to volume for interfacial charge collection/separation, ion transport across liquid/solid interfaces (i.e., for mass-transport-limited processes in general) and (ii) a template for depositing nanostructured films of small molecules or polymers that serve as optically and electronically active layers for these devices. In addition, while there have been many efforts to fabricate nanostructures of ITO (the most popular transparent conducting oxide for use in such devices) [81–89], templated shadow evaporation is the first to produce uniform, free-standing ordered arrays of electrically connected ITO nanotubes with controllable dimensions.

As a nanostructured shadow mask, we used a nonlithographic template: a commercially available anodized alumina (AAO) membrane (Whatman Anodisc; 60 μm thick, 200 nm diam. pores). These membranes dissolve easily in aqueous base and have a high density (~10^9–10^{11} cm^{-2}) of straight pores with monodisperse diameters. Alumina membranes with regular, cylindrical pores with diameters from 10 nm to microns can also be fabricated through established anodic processing techniques.

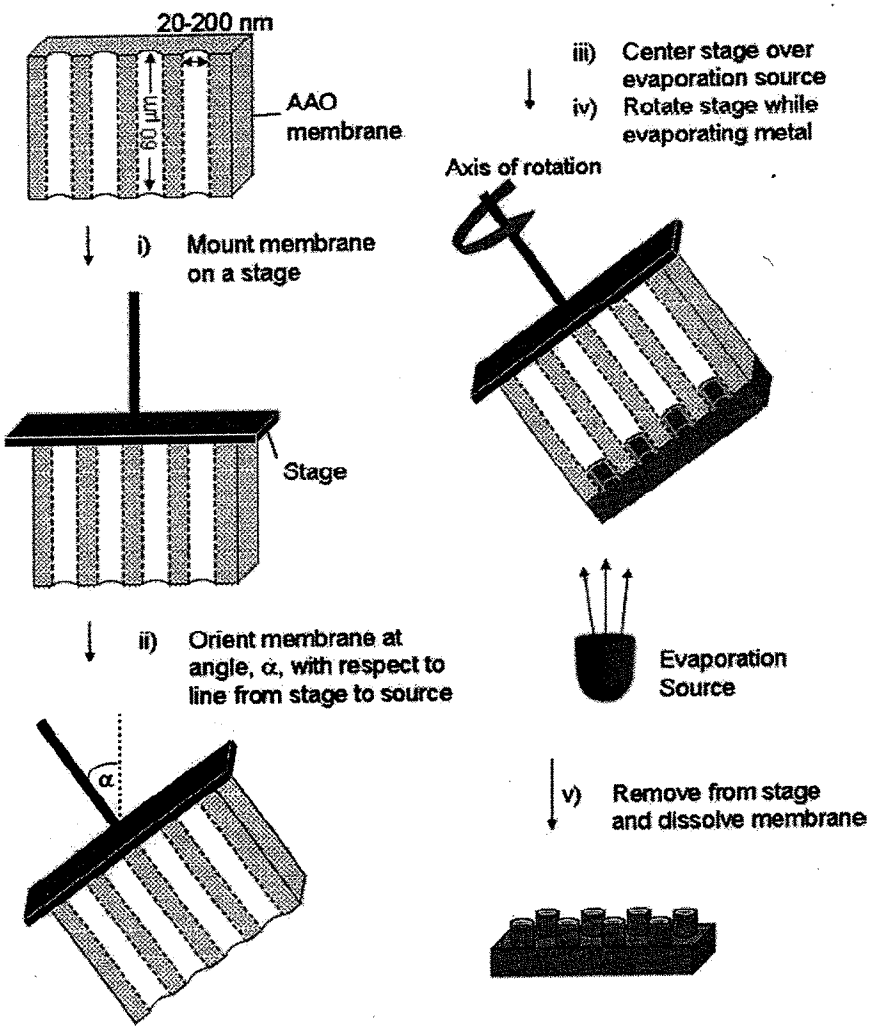

Figure 10.19 Procedure for fabrication of nanotube arrays: We (i) mounted an anodized alumina (AAO) membrane onto a stage, (ii, iii) centered the stage directly above the evaporation source at an incident angle α, defined as the angle between the axis of rotation and a line drawn from the source to the AAO membrane) and (iv) evaporated onto the membrane. The edges of the pores of the membrane cast shadows into the pores. (v) We immersed the coated membrane in 1 M NaOH to completely etch the AAO membrane and yield an array of nanotubes connected by a continuous backing of the same material. Reprinted with permission from [17]. Copyright 2007, American Chemical Society.

Figure 10.19 shows the general procedure for fabricating arrays of nanotubes. We mounted the membrane flush against a rotating plate driven by a battery-powered DC motor and e-beam evaporated ~150 nm of metal (Au or Pt) or ITO onto the membrane. We fixed the evaporation incident angle (α) between 0 and 90° to control the height of the nanotubes. After deposition, we removed the AAO membrane from the rotating support. The alumina dissolved when the AAO–metal (or ITO) composite was immersed in aqueous base. This procedure yielded an array of nanotubes supported by an electrically continuous backing of the same material.

In principle, the technique we describe is compatible with any material that can be vapor-deposited, either through thermal or e-beam evaporation. Electron-beam evaporation is the preferred method for this particular technique because, in contrast to other evaporation techniques (e.g., sputtering), the evaporating material produced by an electron beam has a long mean free path due to the low pressure in the chamber (~1×10^{-6} torr; n.b., 1 torr = 133 Pa) and, thus, is approximately collimated after traveling from the source to the substrate (~45 cm total distance). The collimated beam is critical for this application because the shadows cast by the AAO membrane into its pores defines the geometry of the tubes.

The heights of the structures depended on the angle of evaporation (α, the angle between the axis of rotation and a line between the source and the AAO membrane). Figure 10.19 shows micrographic evidence of the dependence of height of Au tubes on incident angle of evaporation for the two most extreme angles (0°, 90°), and an intermediate angle (45°). At a glancing angle (Figure 10.20a, $\alpha \sim 90°$), the Au structures formed a loosely connected array of rings, because the collimated beam did not penetrate the pores, and only a small amount of deposited material adhered to the membrane. The diameter of the rings was approximately 200 nm (the diameter of the pores of the AAO membrane). At $\alpha \sim 45°$ (Figure 10.20b), the tubes formed structures whose height was approximately the same as their diameter (~200 nm). At a normal angle (Figure 10.20c, $\alpha \sim 0°$), the structures formed an array of long nanotubes (~1.5 μm tall). These are the highest aspect ratio nanotubes formed using a one-step physical vapor deposition process on AAO membranes. The walls of the tubes, however, were thin since the collimated beam projected parallel to the walls of the pores. Many of the tubes in Figure 10.20c therefore mechanically separated from the substrate or collapsed during sample preparation.

10.2.4.2 **Outlook**

In photolithography (and most other methods of pattern transfer), the fabricated structure has a one-to-one correspondence to the master structure. Shadow evaporation is unique because the information is encoded in the three-dimensional topography of the master. This "line-of-sight" deposition allows for an infinite number of possible structures or patterns to be fabricated using the same master simply by changing the angle of the substrate with respect to the source. Shadow evaporation, therefore, increases the effective complexity of a topographically patterned master by introducing the angle as another variable that is capable of rendering different product structures.

The technique is potentially conservative with respect to energy because the same master structure can be used with different angles and source materials to generate multicomponent structures. While photolithography is typically used for pattern transfer in two dimensions, the heights of the individual photoresist features may be exploited in shadow evaporation. In fact, electronic components such as resistors, capacitors, and metal oxide semiconductor field-effect transistors (MOSFETs) can be formed using only a single layer of photolithography on a silicon wafer [90].

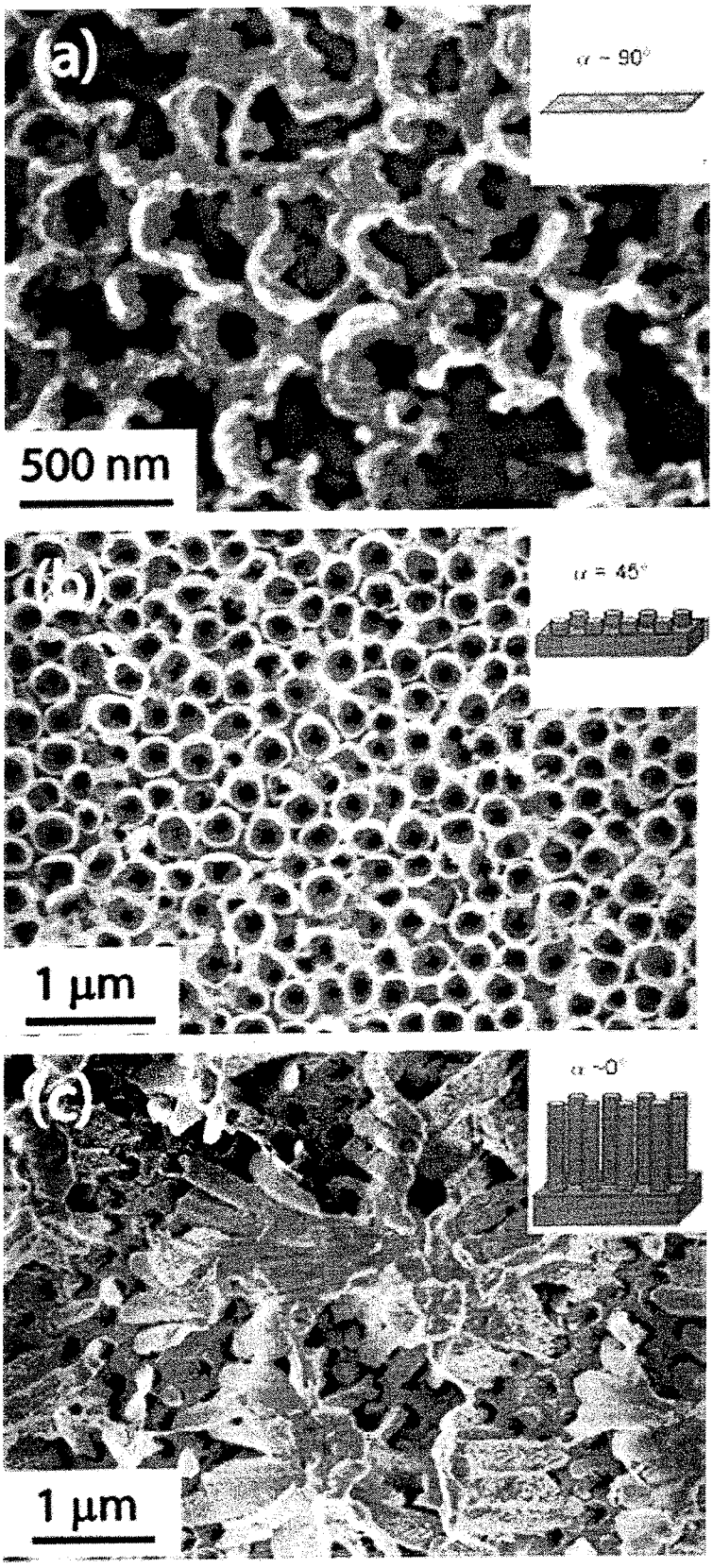
(a)
α = 90°
500 nm
(b)
α = 45°
1 μm
(c)
α ~0°
1 μm

Figure 10.20 SEM images (top view) of Au nanostructures formed at various incident angles α (insets: the corresponding oblique-angle schematic diagrams illustrating the dependence of the ideal geometry of the nanotube on α for a given amount of deposited material). (a) α ~ 90° (glancing): an array of small rings formed with a minimal backing layer. The collimated evaporation source resulted in negligible penetration into the pores and a thin backing layer. (b) α ~ 45°: an array of short tubes formed. (c) α ~ 0° (normal): an array of tall, thin-walled tubes formed with a thick backing layer. The penetration was deep into the pores, but the walls of the tube were thin because collimation of the vaporized material was parallel to the pores. Reprinted with permission from [17]. Copyright 2007, American Chemical Society.

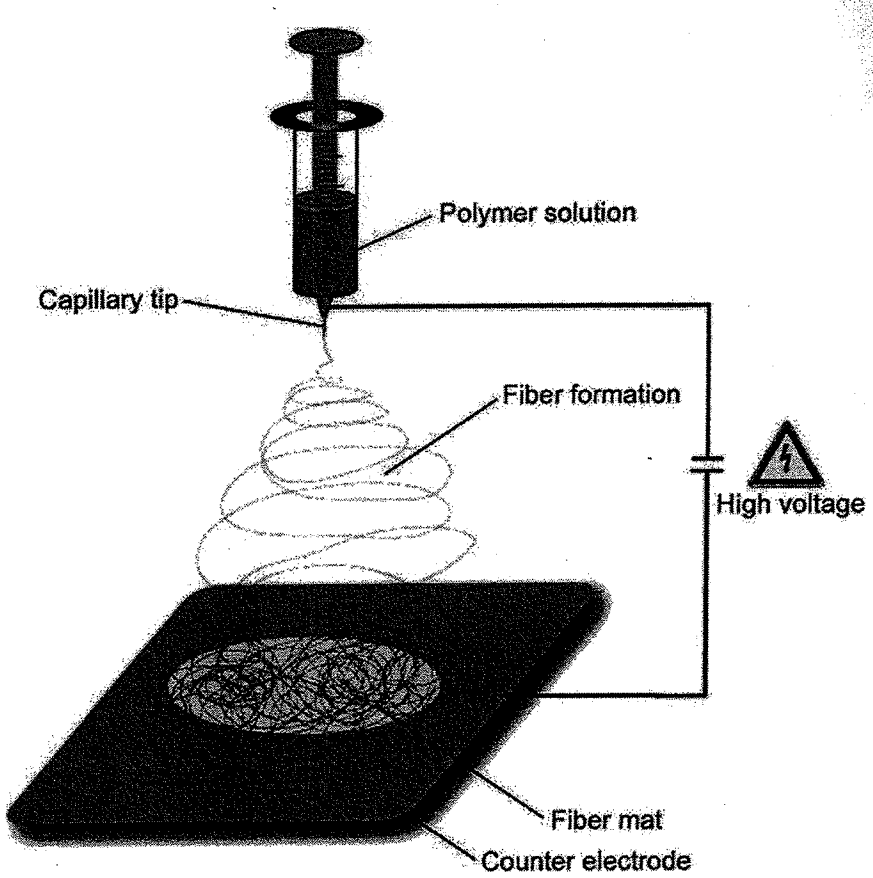

Figure 10.21 Schematic illustration of the electrospinning process. Reprinted with permission from [92]. Copyright 2007, Wiley-VCH Verlag GmbH & Co. KGaA.

10.2.5 Electrospinning

Electrospinning is a technique for making nanofibers of a range of organic and inorganic materials by the electrostatic extraction of a solid fiber from a solution or melt [91]. While it has been reviewed before [92], we focus on the newest developments, which include methods to produce aligned and multicomponent nanofibers. The typical setup is depicted in Figure 10.21. A syringe containing a

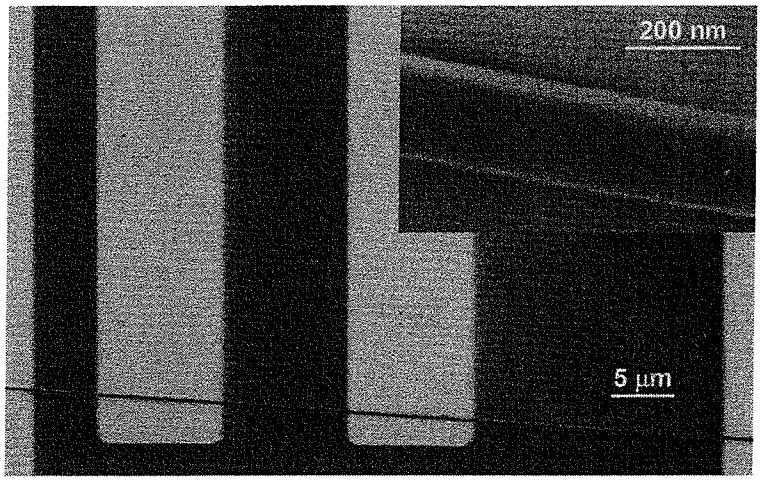

Figure 10.22 A single electronspun fiber of P3HT spanning microfabricated electrodes on an Si/SiO_2 substrate. The inset is a closeup of the fiber. The nanofiber behaves as a field-effect transistor. Reprinted with permission from [74]. Copyright 2005, American Institute of Physics.

solution-based precursor is held at a high voltage (10–50 kV). A drop of solution is extruded from the needle or capillary from which a jet is electrostatically ejected toward a grounded substrate platform. As the jet of material reaches the substrate, the solvent evaporates or the material otherwise hardens to form a continuous fiber. In the typical case, the deposition of the fiber is not controlled, so it forms a disordered mat on the substrate. We restrict our attention to modifications of the electrospinning technique that generate aligned nanofibers and those that generate multicomponent core-shell or hollow nanofibers.

10.2.5.1 Scanned Electrospinning

Craighead and coworkers have developed a procedure that produces single nanofibers of polymers by a scanned electrospinning process [93]. In this procedure, a microfabricated spinneret is dipped in a solution and held in close proximity (*ca.* 2 cm) from the grounded substrate. The jet originates from the sessile drop attached to the spinneret. The key to scanned electrospinning is a motor that translates the substrate during the spinning process. The relative motion of the substrate with respect to the spinneret allows fibers to be deposited in a predictable orientation. The use of photolithographically patterned electrodes on the substrate platform enables the characterization of single-nanowire devices. For example, a chemical sensor based on polypyrrole [78] and an organic field-effect transistors (OFETs) based on poly(3-hexylthiophene) (P3HT) have been demonstrated (Figure 10.22) [74]. In the case of the P3HT nanowire OFET, the measured charge carrier mobility was comparable to those found in devices based on thin films. This result suggests that electrical properties of the P3HT were intact after the electrospinning process. With greater control, scanned electrospinning might become useful for nanoelectronic applications; it is already useful as a low-energy method for making electronic test structures in academic laboratories.

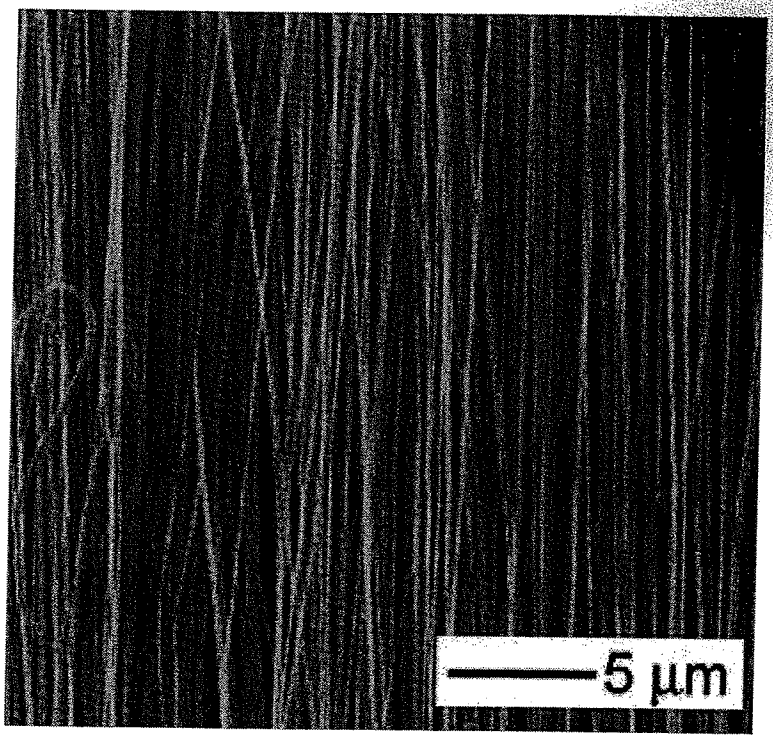

Figure 10.23 Uniaxially oriented $BaTiO_3$ nanofibers fabricated by electrospinning over an insulating gap between a metal electrodes. Reprinted with permission from [98]. Copyright 2006, Elsevier.

10.2.5.2 Uniaxial Electrospinning

Self-assembly of nanofibers as they are extruded from the spinneret is another route that is being investigated for control over the electrospinning process. For example, Xia and coworkers are developing a model for the ways in which electric fields influence the orientation of nanofibers on a substrate [94–97]. They have found that the presence of insulating shapes patterned on an otherwise conductive surface direct the formation of parallel nanofibers. Figure 10.23 shows uniaxial collections of barium titanate nanofibers.

10.2.5.3 Core/Shell and Hollow Nanofibers

Multicomponent nanofibers in a core/shell geometry have also been demonstrated for several combinations of materials (Figures 10.24 and 10.25) [100, 101]. This process is performed with a compound spinneret, in which a smaller needle is placed inside a larger needle. Electrospinning from this arrangement causes the jet to have a core/shell of two different polymers. For example, conjugated polymers have been placed in the interior of fibers made of poly(vinylpyrrolidone) (PVP) [102]. Two conjugated polymers together may also serve as the core and shell at the same time [101]. Such heterostructures could find use in optoelectronic applications. The inner spinneret can also contain a sacrificial material, such as mineral oil, which upon rinsing may be removed to form hollow nanofibers [102].

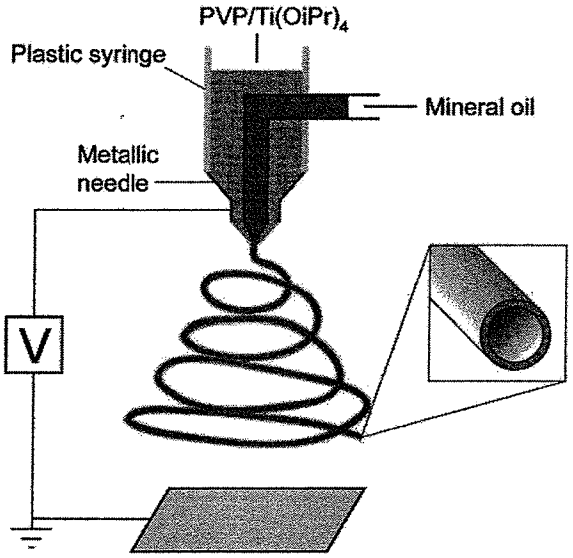

Figure 10.24 Schematic illustration of the compound spinneret used to generate core-shell multicomponent polymer nanofibers. Reprinted with permission from [99]. Copyright 2005, Royal Society of Chemistry.

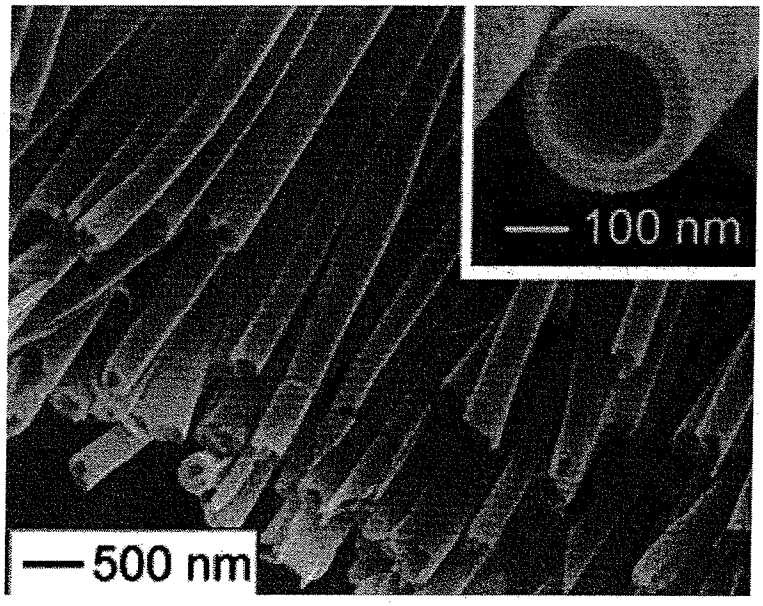

Figure 10.25 Hollow nanofibers of aligned anatase TiO_2 collected across an insulating gap on a conductive substrate. The cross-sections of the fibers were exposed using a razor blade. Reprinted with permission from [99]. Copyright 2004, American Chemical Society.

10.2.5.4 Outlook

The electrospinning phenomenon is remarkable in its applicability to most materials that can be processed from melt or solution. The basic function of electrospinning is to deposit randomly oriented mats of fibers. The challenge is to deposit single nanowires or oriented collections of nanofibers. Some combination of stage translation and electrostatic self-assembly might enable the eventual integration of electrospun fibers into nanoscale devices.

The energetic costs associated with electrospinning are low. A typical high-voltage DC power supply drains about 10 W in normal operation. Scanned electrospinning also requires an electric motor to translate the stage, which typically draw <100 W. The in-flight, uniaxial assembly of nanofibers as described by Xia and coworkers requires conductive and insulating zones patterned on a substrate [95].

10.2.6 Self-Assembly

Self-assembly (SA) is a ubiquitous strategy in nanofabrication [22, 103]. It is the spontaneous organization of one or more components using covalent or noncovalent interactions into ordered superstructures. There are elements of SA in the chemical synthesis of nanocrystals and their organization into superlattices, the formation of Langmuir–Blodget films and of course the tertiary structure of proteins. An entire organism is an example of dynamic SA [22]. The operation of a cell relies on precisely evolved nanostructures, which are much more complex than any manmade system. Thus, biology provides proof-of-principle of the potential utility and efficiency of SA. In the context of green nanofabrication, SA is potentially an elegant strategy, if the assembly step occurs under sufficiently mild conditions.

Two types of SA are important to fabrication: nontemplated and templated [1]. Nontemplated self-assembly is the purest form. It relies only on the interactions of the individual components with each other, without external forces and spatial constraints. Materials that are assembled this way include nanoparticles, SAMs and structures that assemble from liquid crystals and block copolymers. The most appealing aspect of nontemplated self-assembly is that, ideally, the only energetic inputs are those of the synthesis of the individual components. While nontemplated SA is presently only able to generate a limited set of structures, it has significant potential. Templated SA relies on external forces and spatial constraints of a rationally designed master structure, which is usually derived from a top-down process. An example of a combination of templated and nontemplated strategies is the use of patterned substrate to increase the length of ordering in a block copolymer film [104].

The ubiquity of SA in nanofabrication precludes a thorough treatment of the subject here. We direct the reader to the book by Ozin and Arsenault for an excellent review of SA and other chemical approaches to nanotechnology [105]. The rest of this section will focus on two examples of SA: stacked films of semiconductor

nanocrystal superlattices and block copolymer lithography. These two examples also have potential applications in the conversion and storage of energy.

10.2.6.1 Hierarchical Assembly of Nanocrystals

One of the simplest routes to manufacturing nanomaterials on a large scale is solution-phase, bulk chemical synthesis. The energetic costs associated with these "wet" processes are the same as those associated with ordinary chemical synthesis: chemical precursors, solvents, temperature control and ventilation. A large number of syntheses are available for metallic and semiconducting nanocrystals and carbon nanotubes [106]. These processes are successful in bulk applications where they are used as ordinary chemical reagents. For academic purposes, randomly oriented, individual nanostructures are selected from a collection and characterized (electronically or optically). The extent to which structures from wet chemical synthesis can be integrated into devices depends on the ease with which single nanostructures can be deposited on predefined locations with a high density. Chemical synthesis produces nanostructures in the solution phase, so they can be deposited on any substrate they will stick to, including low-cost substrates like plastic and metallic foil, by a variety of bench-top techniques (spin-coating, dip-coating, printing, etc.) and in a variety of thicknesses and interparticle spacings.

Wet chemical synthesis can produce macroscopic quantities of semiconductor quantum dots with narrow polydispersities. The average size of the dots can be selected by slightly altering the conditions of the synthesis. For instance, many groups [97, 107–113] now routinely synthesize monodisperse ($\sigma < 4\%$ rms) colloidal CdSe quantum dots (QDs) at temperatures less than 400 °C using wet-chemical procedures. The QDs have diameters ranging from 1.2 to 15.0 nm (the bulk exciton radius of CdSe is ~5 nm [114]), good electronic passivation and uniform shape [107, 115, 116]. These synthetic methods make CdSe QDs useful and highly developed building blocks for the fabrication of superlattices ordered over hundreds of microns [117–120], with controllable nearest neighbor distances [117, 121]. Furthermore, CdSe QDs have a finely tuned profile of absorption versus size with good coverage of the visible spectrum: for d = 1.2 nm to 15 nm, the band gap (E_g) ranges from 2.9 eV (~425 nm) to 1.75 eV (~710 nm) [107, 117, 121–125].

Our group produced three different sizes of CdSe QDs in order to construct junctions of three-dimensional arrays containing CdSe QDs of multiple sizes (Figure 10.26). The arrays of QDs are hierarchically self-assembled: first, atoms into the dots themselves and then the dots into polycrystalline superlattices. These superlattices are stacked using spin-coating, which introduces an additional level of complexity to the composite film. These multi-size arrays enabled us to infer some of the electronic consequences of quantum confinement that have been largely unexplored and unexploited in devices based on QDs: the importance of energetic alignment of the orbitals of the QDs and the work functions of the electrodes [127, 128] in determining the electrical characteristics of the junctions.

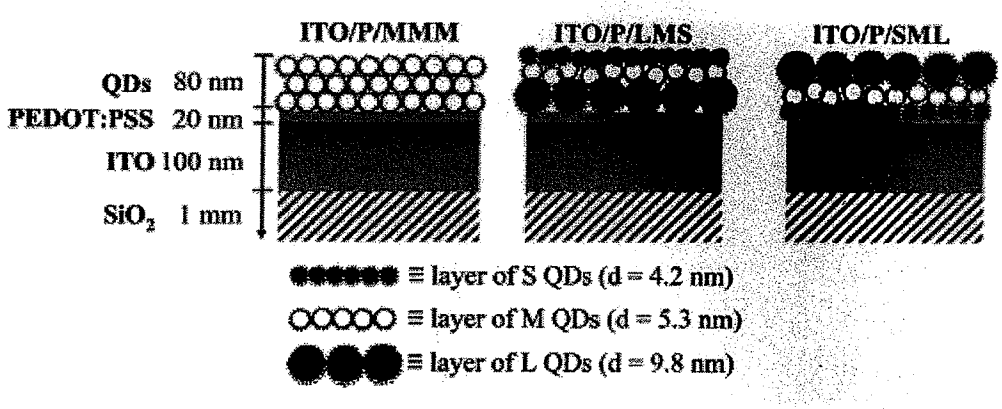

Figure 10.26 Schematic diagrams of selected films of QDs on ITO/PEDOT:PSS: ITO/P/MMM, ITO/P/LMS, and ITO/P/SML. "S," "M," and "L" indicate small (d = 4.2 nm), medium (d = 5.3 nm), and large (d = 9.8 nm) CdSe QDs, respectively, and "P" indicates a ~20 nm layer of polymer. Each monolayer of QDs in the diagram represents a multilayer (25–30 nm thick) in the actual film. Reprinted with permission from [126]. Copyright 2008, American Chemical Society.

10.2.6.2 Block Copolymers

Recent advances in polymer synthesis and an increased understanding of the physics of block copolymers have led to their incorporation in microelectronics applications [104]. Block copolymer chains contain two or more covalently linked, chemically distinct segments. These compounds form complex structures in the solid phase because of preferential association of chemically similar blocks minimizes the free energy of the system. Covalent linkage of the two blocks in a copolymer prevents long-range phase segregation of the two components, which occurs in blends of two or more homopolymers. Instead, block copolymers self-assemble into microdomains. These microdomains are nanometric features that can be used directly or as a template to direct further elaboration of the substrate [129].

One of the most useful morphologies of a block copolymer thin film has cylindrical microdomains of the minor block with their axes perpendicular to the substrate. Thin films of polystyrene-*block*-poly(ethylene oxide) (PS-*b*-PEO) spin-coated on a silicon wafer and annealed in a vapor of benzene can produce laterally ordered arrays of hexagonally packed cylinders with grain sizes of tens of square microns (Figure 10.27) [130]. This technique is known as solvent-induced ordering, which is a key to long-range self-assembly of block copolymer films [104].

Block copolymer lithography is the transfer of the thin film morphology of a block copolymer to another surface. This process is usually accomplished by selective etching of the minor component to reveal a nanoporous array. The nanoporous film then may be used directly, or serve as a pattern transfer element (as a mask or a template). In some sense, block copolymer templates are analogous to anodic aluminum oxide templates, though block copolymer films can have a higher density of features [104].

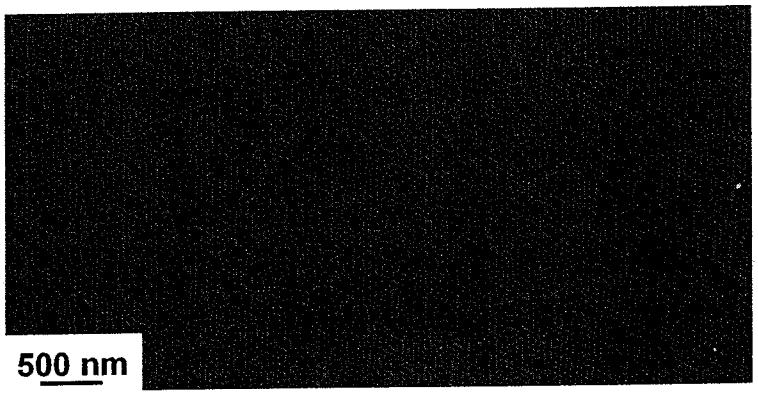

Figure 10.27 Scanning force micrograph of a highly ordered array of hexagonally packed cylindrical microdomains in a thin film of PS-b-PEO. Reprinted with permission from [130]. Copyright 2004, Wiley-VCH Verlag GmbH & Co. KGaA.

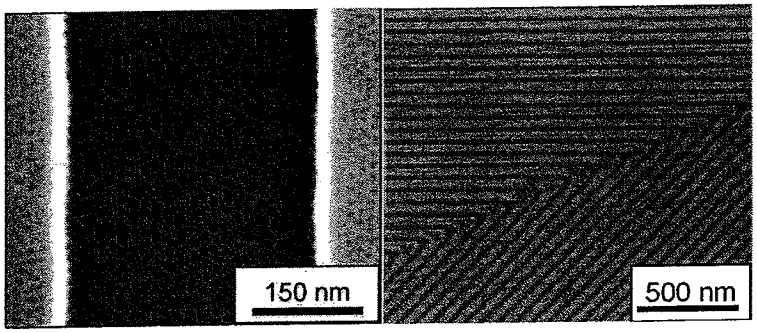

Figure 10.28 Two types of epitaxial self-assembly of block copolymer films. (Left) A trench etched in a SiO_2 substrate directs the orientation of the grains in a film of poly(α-methylstyrene)-*block*-poly(4-hydroxystyrene) film. Reprinted with permission from [131]. Copyright 2008, American Chemical Society. (Right) A chemically patterned surface directs the orientation of domains in a ternary blend of PS-*b*-PMMA, PS, and PMMA. The chemically patterned lines are commensurate with the natural lamellar period of the block copolymer film. Homopolymers are recruited to the points of discontinuity (the bends) in the lines. Reprinted with permission from [133]. Copyright 2005, American Association for the Advancement of Science.

For many applications, it is not sufficient that a block copolymer film display simple periodicity. Electronic devices require the ability to produce arbitrary patterns. In various techniques of epitaxial deposition, a lithographically patterned surface can direct the formation of self-assembled structures. This underlying pattern can be of a topographic [131] or chemical nature [132]. Topographic patterns can affect the long-range periodicity and the morphology of microdomains perpendicular to the substrate (nanodots) within trenches. Chemical patterning can direct the formation of patterns of block copolymer films in which the microdomains lie parallel to a chemically patterned surface. Figure 10.28 shows examples of these two types of hierarchical ordering. Chemical patterning of surfaces

with a periodicity close to that of the bulk lamellar spacing of a block copolymer film can cause the lamellae to follow angular discontinuities. While the lamellae can become strained and discontinuous when coerced to follow angles on a patterned substrate, added homopolymers can be recruited to the sites of discontinuities and alleviate the strain. In this way, Nealey and coworkers were able to overlay a ternary blend of the diblock copolymer polystyrene-*block*-poly(methylmethacrylate) (PS-*b*-PMMA) and homopolymers of PS and PMMA atop a chemically patterned surface in which the lamellae were physically continuous over bends in the substrate.

10.2.6.3 Outlook

Self-assembly is progressing as an approach to nanofabrication, though in its nontemplated form it does not yet possess the capability of producing structures as complex as those available to top-down techniques [1]. Templated systems mix "top-down" with "bottom-up" methods of nanofabrication. Epitaxial self-assembly makes it possible to integrate block copolymer structures with conventional lithographic patterns. We are optimistic that the role of self-assembly for nanofabrication will increase in the future, especially because of the potential for fabrication in three dimensions, the opportunity for reversible [134] self-assembly and the possibility that self-assembled structures can self-repair or self-replicate [135].

10.3 Future Directions: Toward "Zero-Cost" Fabrication

This section describes three examples of extremely low-cost fabrication: the use of Scotch tape to fabricate islands of graphene monolayers [136] paper as an extremely low-cost substrate for microfabrication [137, 138] and Shrinky-Dinks as a photoresist substitute for soft lithography mastering [139, 140]. While not necessarily "nano", these techniques are salient examples of simplicity in fabrication and are perfectly suitable for low-cost (and low-energy) academic research. These methods demonstrate that even the simplest of techniques can yield potentially important advances: the Scotch-tape method led to the experimental discovery of graphene [136]; patterning paper as a substrate for microfabrication has potential for manufacturing portable bioassays for developing countries [138]; and printing on biaxially prestressed polymeric substrates could lead to an inexpensive, non-photolithographic method of miniaturizing printed features [139, 140].

10.3.1 Scotch-Tape Method for the Preparation of Graphene Films

Graphene is a two-dimensional monolayer of carbon atoms packed into an infinite array of fused benzene rings. Fullerenes, carbon nanotubes, and graphite can be regarded as zero-, one- and three-dimensional arrangements of graphene sheets

[141]. For half a decade, graphene was considered too unstable to exist, and was only studied theoretically. In 2004, Novoselov et al. discovered the first atomically thin carbon films using an astonishing combination of simple tools: scotch tape and an optical microscope [136]. Scotch tape was used to cleave individual graphene planes off of bulk graphite, and the characteristic optical interference patterns of graphene layers on an Si/SiO_2 wafer of the appropriate oxide thickness allowed the flakes of atomic thickness and microscopic width to be visualized (scanning-probe microscopy and SEM techniques were unable to find the specimens). Since that time, there has been an explosion of reports in the literature on experimental studies of graphene that have verified theoretical models and demonstrated the potential utility of the material for applications in nanoscale electronics.

10.3.2
Patterned Paper as a Low-Cost Substrate

Our group has published a method for patterning paper to create well-defined, millimeter-sized channels, comprising hydrophilic paper bounded by hydrophobic polymer (see Figure 10.29, left panel) for details of the fabrication process) [137, 138]. This type of patterned paper could be used for low-cost, portable and technically simple multiplexed bioassays (Figure 10.29, right panel). We made assay devices based on paper by patterning photoresist onto chromatography paper to form defined areas of hydrophilic paper separated by hydrophobic lines or walls; these patterns provide spatial control of biological fluids and enable fluid transport owing to capillary action in the millimeter-sized channels. In a fully developed technology, patterned photoresist would be replaced by an appropriate printing technology.

10.3.3
Shrinky-Dinks for Soft Lithography

While the various forms of soft lithography have been adopted by a large number of research laboratories, most incarnations of the technique require access to modern photolithographic equipment (mask aligners, etc.) and materials (photoresists, wafers, etc.). Khine and coworkers have recently developed tools for soft lithography based on the childrens' toys "Shrinky-Dinks." Shrinky-Dinks are biaxially prestressed polystyrene thermoplastic sheets. When heated, the sheets contract laterally by approximately 63% with a concomitant increase in height of features printed on the substrate by 500% [140]. Recessed features also become deeper. These characteristics were used in the mastering [140] and direct fabrication [139] of microfluidic devices.

In a first demonstration, a laser printer was used to pattern lines on sheets of prestressed polystyrene [140]. Upon heating, the substrate contracted while the printed features of ink were raised. PDMS was then poured over the polystyrene/ink master and cured (Figure 10.30a). The PDMS stamp bonded easily to a glass

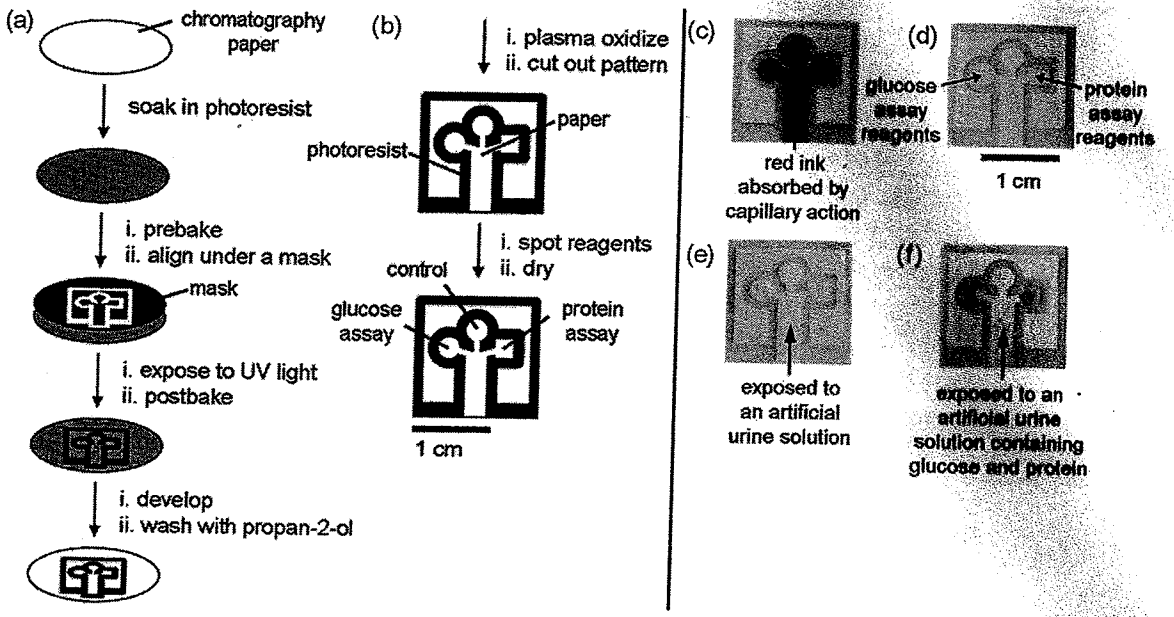

Figure 10.29 (Left) Diagram depicting the method for patterning paper into millimeter-sized channels: (a) Photolithography was used to pattern SU-8 photoresist embedded into paper, (b) the patterned paper was modified for bioassays. (Right) Chromatography paper patterned with photoresist. Darker lines are cured photoresist, whereas lighter areas are unexposed paper. (c) Patterned paper after absorbing Waterman red ink (5 μL) by capillary action. The central channel absorbs the sample by capillary action and the pattern directs the sample into three separate test areas. (d) Complete assay after spotting the reagents. The square region on the right is the protein test and the circular region on the left is the glucose test. The circular region on the top was used as a control well. (e) Negative control for glucose (left) and protein (right) by using an artificial urine solution (5 μL). (f) Positive assay for glucose (left) and protein (right) by using a solution that contained 550 mM glucose and 75 μM BSA in an artificial urine solution (5 μL). The control well was spotted with potassium iodide solution, but not with enzyme solution. Reprinted with permission from [137]. Copyright 2007, Wiley-VCH Verlag GmbH & Co. KGaA.

slide to form complex patterns of microchannels (with a maximum height of 80 μm) through which cells could flow. Iterative printing could increase the heights of features. Multiple heights of features—which are difficult to obtain with conventional photolithographic mastering—could be obtained by printing over selected features of the master. The minimum linewidth was 63 μm, but the authors suggest that a higher-resolution printer could achieve a smaller value.

In a second demonstration, the polystyrene itself was scribed manually with lines using a hypodermic needle [139]. Several complementary designs were stacked and shrunk together to form an interconnected, three-dimensional microfluidic device. In a manufacturing setting, the manual scribing step would be replaced by an automated indentation tool. A photograph of a test structures appears in Figure 10.30b. Microfluidic devices based on PDMS are amenable to

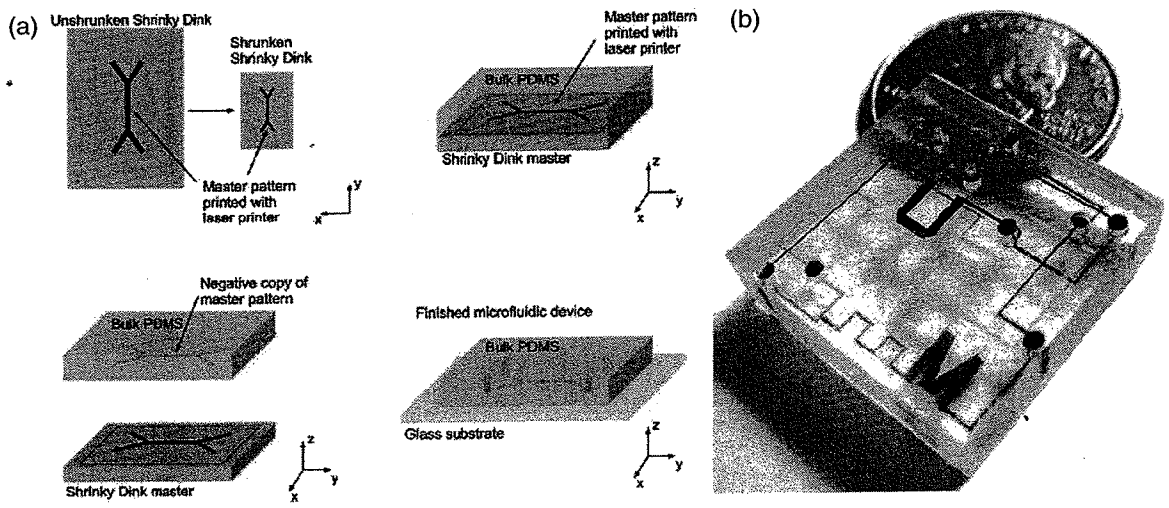

Figure 10.30 (a) Schematic illustration of the use of printed Shrinky-Dinks as masters for soft lithography. (b) Photograph of a three-dimensional, all-polystyrene microfluidic device, which contains three layers (separate networks of channels). Reprinted with permission from [139] and [140]. Copyright 2008, Royal Society of Chemistry.

rapid prototyping in a research setting, but PDMS is not favored industrially because of issues of swelling and compression [139]. A benefit of the Shrinky-Dink method is that it is amenable to rapid prototyping, while polystyrene is a rigid, industrially viable material.

10.4 Conclusions

Nanostructured materials may contribute to the efficient storage and production of energy, but only if they are produced in environmentally responsible ways. We have described several of the energetic aspects of conventional and unconventional approaches to nanofabrication and several techniques that satisfy many of the criteria for energy conservation. These techniques possess significant potential for test structures in academic laboratories and some offer manufacturing capabilities.

We have two goals in pursuing this topic:

The first, immediate goal is to increase awareness among researchers of the design constraints for green nanofabrication. Major universities are already taking the lead in reduction of greenhouse gas emissions. In 2008, an anonymous university taskforce reported that the university emits 282 000 t year^{-1} of carbon dioxide equivalents. The electricity bill of the nanofabrication facility, alone, accounts for about 2% of the energy budget of the entire university. We hope that, by characterizing some of the successes of unconventional approaches to nanofabrication, we have shown that simple tools and materials can often yield functionally equivalent

structures to those made by conventional techniques. In many cases, combining the re-use of an existing tool with the exploitation of nanoscale information in unconventional sources can yield totally unique structures. We expect that green nanofabrication could find immediate use for the fabrication of test structures in a research setting, as well as forestall regulations on nanoscience based on the costs of performing experiments in this often energy-intensive area of research.

The second, long-term goal is to promote the development of green approaches to nanofabrication that have some potential for manufacturing. It is understood that integrating a new approach into an established field, such as microelectronics, is hindered by the risks of tampering with an existing infrastructure. We expect that green approaches to semiconductor manufacturing, such as the use of supercritical CO_2 and block copolymer lithography, will continue to decrease the energy intensity of the industry. Green techniques, however, have the characteristic that their products are perhaps the most relevant to emerging fields–areas outside of microelectronics that do not yet posses an infrastructure for manufacturing.

Acknowledgments

This research was supported by the United States Department of Energy under DE-FG02-00ER45852 and the National Science Foundation under CHE-0518055. D.J.L. acknowledges a graduate fellowship from the American Chemical Society, Division of Organic Chemistry, sponsored by Novartis. E.A.W. thanks the Petroleum Research Fund of the American Chemical Society fellowship (PRF no. 43083-AEF). The authors thank Noah Clay and Jiangdong Deng (Harvard) for helpful discussions.

References

1 Gates, B.D., Xu, Q.B., Stewart, M., Ryan, D., Willson, C.G., and Whitesides, G.M. (2005) *Chem. Rev.*, **105**, 1171.

2 Arakawa, H., Aresta, M., Armor, J.N., Barteau, M.A., Beckman, E.J., Bell, A.T., Bercaw, J.E., Creutz, C., Dinjus, E., Dixon, D.A., Domen, K., DuBois, D.L., Eckert, J., Fujita, E., Gibson, D.H., Goddard, W.A., Goodman, D.W., Keller, J., Kubas, G.J., Kung, H.H., Lyons, J.E., Manzer, L.E., Marks, T.J., Morokuma, K., Nicholas, K.M., Periana, R., Que, L., Rostrup-Nielson, J., Sachtler, W.M.H., Schmidt, L.D., Sen, A., Somorjai, G.A., Stair, P.C., Stults, B.R., and Tumas, W. (2001) *Chem. Rev.*, **101**, 953.

3 Yang, S.Y., Ryu, I., Kim, H.Y., Kim, J.K., Jang, S.K., and Russell, T.P. (2006) *Adv. Mater.*, **18**, 709.

4 Garcia, E.J., Hart, A.J., Wardle, B.L., and Slocum, A.H. (2007) *Adv. Mater.*, **19**, 2151.

5 Whitesides, G.M., and Crabtree, G.W. (2007) *Science*, **315**, 796.

6 O'Neil, A., and Watkins, J.J. (2004) *Green Chem.*, **6**, 363.

7 National Association of Manufacturers (2008) Facts About U.S. Manufacturing, http://www.nam.org/s_nam/bin.asp?CID=202325&DID=233605&DOC=FILE.PDF (accessed 13 July 2008).

8 Williams, E.D., Ayres, R.U., and Heller, M. (2004) *Environ. Sci. Technol.*, **38**, 1916.

9 Williams, E.D., Ayres, R.U., and Heller, M. (2002) *Environ. Sci. Technol.*, **36**, 5504.

10 Williams, E. (2004) *Environ. Sci. Technol.*, **38**, 6166.

11 Shadman, F., and McManus, T.J. (2004) *Environ. Sci. Technol.*, **38**, 1915.

12 Hu, S.C., Wu, J.S., Chan, D.Y.L., Hsu, R.T.C., and Lee, J.C.C. (2008) *Energy Build.*, **40**, 1765.

13 Hu, S.C., and Chuah, Y.K. (2003) *Energy*, **28**, 895.

14 Ginger, D.S., Zhang, H., and Mirkin, C.A. (2004) *Angew. Chem. Int. Ed.*, **43**, 30.

15 Xu, Q., Rioux, R.M., and Whitesides, G.M. (2007) *ACS Nano*, **1**, 215.

16 Xu, Q.B., Gates, B.D., and Whitesides, G.M. (2004) *J. Am. Chem. Soc.*, **126**, 1332.

17 Dickey, M.D., Weiss, E.A., Smythe, E.J., Chiechi, R.C., Capasso, F., and Whitesides, G.M. (2008) *ACS Nano*, **2**, 800.

18 Aizenberg, J., Black, A.J., and Whitesides, G.M. (1998) *Nature*, **394**, 868.

19 Lipomi, D.J., Chiechi, R.C., Dickey, M.D., Whitesides, G.M., and Nano, L. (2008) *Nano Lett.*, **8**, 2100.

20 Xu, Q.B., Mayers, B.T., Lahav, M., Vezenov, D.V., and Whitesides, G.M. (2005) *J. Am. Chem. Soc.*, **127**, 854.

21 Zach, M.P., Ng, K.H., and Penner, R.M. (2000) *Science*, **290**, 2120.

22 Whitesides, G.M., and Grzybowski, B. (2002) *Science*, **295**, 2418.

23 Gur, I., Fromer, N.A., Geier, M.L., and Alivisatos, A.P. (2005) *Science*, **310**, 462.

24 Menard, E., Meitl, M.A., Sun, Y.G., Park, J.U., Shir, D.J.L., Nam, Y.S., Jeon, S., and Rogers, J.A. (2007) *Chem. Rev.*, **107**, 1117.

25 Goh, C., Coakley, K.M., and McGehee, M.D. (2005) *Nano Lett.*, **5**, 1545.

26 Royal Society of Chemistry (2008) *Green Chemistry*'s Impact Factor Continues to Rise. From http://www.rsc.org/Publishing/Journals/gc/News/2008/ImpactFactor.asp (accessed 13 July 2008).

27 Linder, V., Gates, B.D., Ryan, D., Parviz, B.A., and Whitesides, G.M. (2005) *Small*, **1**, 730.

28 Gates, B.D., Xu, Q.B., Love, J.C., Wolfe, D.B., and Whitesides, G.M. (2004) *Annu. Rev. Mater. Res.*, **34**, 339.

29 Johnson, R.C. (2007) *EE Times*, http://www.eetimes.com/showArticle.jhtml?articleID=199203911 (accessed 8 November 2008).

30 Bratton, D., Yang, D., Dai, J.Y., and Ober, C.K. (2006) *Polym. Adv. Technol.*, **17**, 94.

31 Willson, C.G., and Roman, B.J. (2008) *ACS Nano*, **2**, 1323.

32 Rolland, J.P., Maynor, B.W., Euliss, L.E., Exner, A.E., Denison, G.M., and DeSimone, J.M. (2005) *J. Am. Chem. Soc.*, **127**, 10096.

33 Chou, S.Y., Krauss, P.R., and Renstrom, P.J. (1996) *Science*, **272**, 85.

34 Chou, S.Y., Krauss, P.R., and Renstrom, P.J. (1996) *J. Vac. Sci. Technol., B*, **14**, 4129.

35 Chou, S.Y., Krauss, P.R., and Renstrom, P.J. (1995) *Appl. Phys. Lett.*, **67**, 3114.

36 Stewart, M.D., Johnson, S.C., Sreenivasan, S.V., Resnick, D.J., and Willson, C.G. (2005) *J. Microlith. Microfab. Microsys.*, **4**, 011002.

37 Bailey, T.C., Johnson, S.C., Sreenivasan, S.V., Ekerdt, J.G., Willson, C.G., and Resnick, D.J. (2002) *J. Photopolym. Sci. Technol.*, **15**, 481.

38 Xia, Y.N., McClelland, J.J., Gupta, R., Qin, D., Zhao, X.M., Sohn, L.L., Celotta, R.J., and Whitesides, G.M. (1997) *Adv. Mater.*, **9**, 147.

39 Xia, Y.N., Kim, E., Zhao, X.M., Rogers, J.A., Prentiss, M., and Whitesides, G.M. (1996) *Science*, **273**, 347.

40 Kim, E., Xia, Y.N., Zhao, X.M., and Whitesides, G.M. (1997) *Adv. Mater.*, **9**, 651.

41 Palmieri, F., Adams, J., Long, B., Heath, W., Tsiartas, P., and Willson, C.G. (2007) *ACS Nano*, **1**, 307.

42 Heath, W.H., Palmieri, F., Adams, J.R., Long, B.K., Chute, J., Holcombe, T.W., Zieren, S., Truitt, M.J., White, J.L., and Willson, C.G. (2008) *Macromolecules*, **41**, 719.

43 Xia, Y.N., and Whitesides, G.M. (1998) *Annu. Rev. Mater. Sci.*, **28**, 153.

44 Beh, W.S., Kim, I.T., Qin, D., Xia, Y.N., and Whitesides, G.M. (1999) *Adv. Mater.*, **11**, 1038.

45 Coakley, K.M., and McGehee, M.D. (2004) *Chem. Mater.*, **16**, 4533.
46 Yang, F., and Forrest, S.R. (2008) *ACS Nano*, **2**, 1022.
47 Gur, I., Fromer, N.A., and Alivisatos, A.P. (2006) *J. Phys. Chem. B*, **110**, 25543.
48 Kelly, J.Y., and DeSimone, J.M. (2008) *J. Am. Chem. Soc.*, **130**, 5438.
49 Petros, R.A., Ropp, P.A., and DeSimone, J.M. (2008) *J. Am. Chem. Soc.*, **130**, 5008.
50 Hampton, M.J., Williams, S.S., Zhou, Z., Nunes, J., Ko, D.H., Templeton, J.L., Samulski, E.T., and DeSimone, J.M. (2008) *Adv. Mater.*, **20**, 2667.
51 Biebuyck, H.A., Larsen, N.B., Delamarche, E., and Michel, B. (1997) *IBM J. Res. Dev.*, **41**, 159.
52 Xia, Y.N., and Whitesides, G.M. (1997) *Langmuir*, **13**, 2059.
53 Jacobs, H.O., and Whitesides, G.M. (2001) *Science*, **291**, 1763.
54 Salaita, K., Wang, Y.H., and Mirkin, C.A. (2007) *Nat. Nanotechnol.*, **2**, 145.
55 Piner, R.D., Zhu, J., Xu, F., Hong, S.H., and Mirkin, C.A. (1999) *Science*, **283**, 661.
56 Hong, S.H., Zhu, J., and Mirkin, C.A. (1999) *Science*, **286**, 523.
57 Salaita, K., Wang, Y.H., Fragala, J., Vega, R.A., Liu, C., and Mirkin, C.A. (2006) *Angew. Chem. Int. Ed.*, **45**, 7220.
58 Salaita, K.S., Lee, S.W., Ginger, D.S., and Mirkin, C.A. (2006) *Nano Lett.*, **6**, 2493.
59 Rozhok, S., Piner, R., and Mirkin, C.A. (2003) *J. Phys. Chem. B*, **107**, 751.
60 Xu, Q.B., Bao, J.M., Rioux, R.M., Perez-Castillejos, R., Capasso, F., and Whitesides, G.M. (2007) *Nano Lett.*, **7**, 2800.
61 Wiley, B.J., Lipomi, D.J., Bao, J., Capasso, F., Whitesides, G.M., and (2008) *Nano Lett.*, **8**, 3023–3028.
62 Lipomi, D.J., Chiechi, R.C., Reus, W.F., and Whitesides, G.M. (2008) *Adv. Funct. Mater.*, **18**, 3469.
63 Xu, Q.B., Bao, J.M., Capasso, F., and Whitesides, G.M. (2006) *Angew. Chem. Int. Ed.*, **45**, 3631.
64 Xu, Q.B., Perez-Castillejos, R., Li, Z.F., and Whitesides, G.M. (2006) *Nano Lett.*, **6**, 2163.
65 Xu, Q.B., Rioux, R.M., Dickey, M.D., and Whitesides, G.M. (2008) *Acc. Chem. Res.*, **41**, 1566–1577.
66 Ditlbacher, H., Hohenau, A., Wagner, D., Kreibig, U., Rogers, M., Hofer, F., Aussenegg, F.R., and Krenn, J.R. (2005) *Phys. Rev. Lett.*, **95**, 257403.
67 Kan, C.X., Zhu, X.G., and Wang, G.H. (2006) *J. Phys. Chem. B*, **110**, 4651.
68 Sirringhaus, H., Tessler, N., and Friend, R.H. (1998) *Science*, **280**, 1741.
69 Yu, G., Gao, J., Hummelen, J.C., Wudl, F., and Heeger, A.J. (1995) *Science*, **270**, 1789.
70 Sirringhaus, H., Brown, P.J., Friend, R.H., Nielsen, M.M., Bechgaard, K., Langeveld-Voss, B.M.W., Spiering, A.J.H., Janssen, R.A.J., Meijer, E.W., Herwig, P., and de Leeuw, D.M. (1999) *Nature*, **401**, 685.
71 Chiang, C.K., Fincher, C.R., Park, Y.W., Heeger, A.J., Shirakawa, H., Louis, E.J., Gau, S.C., and Macdiarmid, A.G. (1977) *Phys. Rev. Lett.*, **39**, 1098.
72 Wanekaya, A.K., Chen, W., Myung, N.V., and Mulchandani, A. (2006) *Electroanalysis*, **18**, 533.
73 Cui, Y., Wei, Q.Q., Park, H.K., and Lieber, C.M. (2001) *Science*, **293**, 1289.
74 Liu, H.Q., Reccius, C.H., and Craighead, H.G. (2005) *Appl. Phys. Lett.*, **87**, 253106.
75 Duvail, J.L., Retho, P., Fernandez, V., Louarn, G., Molinie, P., and Chauvet, O. (2004) *J. Phys. Chem. B*, **108**, 18552.
76 Smela, E. (2003) *Adv. Mater.*, **15**, 481.
77 Samitsu, S., Shimomura, T., Ito, K., Fujimori, M., Heike, S., and Hashizume, T. (2005) *Appl. Phys. Lett.*, **86**, 233103.
78 Liu, H.Q., Kameoka, J., Czaplewski, D.A., and Craighead, H.G. (2004) *Nano Lett.*, **4**, 671.
79 McQuade, D.T., Pullen, A.E., and Swager, T.M. (2000) *Chem. Rev.*, **100**, 2537.
80 Ramanathan, K., Bangar, M.A., Yun, M., Chen, W., Myung, N.V., and Mulchandani, A. (2005) *J. Am. Chem. Soc.*, **127**, 496.
81 Aoki, Y., Huang, J., and Kunitake, T. (2006) *J. Mater. Chem.*, **16**, 292.

82 Wan, Q., Song, Z.T., Feng, S.L., and Wang, T.H. (2004) *Appl. Phys. Lett.*, **85**, 4759.

83 Limmer, S.J., Cruz, S.V., and Cao, G.Z. (2004) *Appl. Phys. A: Mater. Sci. Process.*, **79**, 421.

84 Wan, Q., Feng, P., and Wang, T.H. (2006) *Appl. Phys. Lett.*, **89**, 123102/1.

85 Cheng, Z.-X., Dong, X.-B., Pan, Q.-Y., Dong, J.-C., and Zhang, X.-W. (2006) *Mater. Lett.*, **60**, 3137.

86 Xue, X.Y., Chen, Y.J., Liu, Y.G., Shi, S.L., Wang, Y.G., and Wang, T.H. (2006) *Appl. Phys. Lett.*, **88**, 201907/1.

87 Jang, H.S., Kim, D.-H., Lee, H.-R., and Lee, S.-Y. (2005) *Mater. Lett.*, **59**, 1526.

88 Yu, D., Wang, D., Yu, W., and Qian, Y. (2003) *Mater. Lett.*, **58**, 84.

89 Orlandi, M.O., Aguiar, R., Lanfredi, A.J.C., Longo, E., Varela, J.A., and Leite, E.R. (2004) *Appl. Phys. A: Mater. Sci. Process.*, **80**, 23.

90 Dickey, M.D., Russell, J.K., Lipomi, D.J., and Whitesides, G.M. (2009) Manuscript in preparation.

91 Reneker, D.H., and Chun, I. (1996) *Nanotechnology*, **7**, 216.

92 Greiner, A., and Wendorff, J.H. (2007) *Angew. Chem. Int. Ed.*, **46**, 5670.

93 Kameoka, J., Czaplewski, D., Liu, H.Q., and Craighead, H.G. (2004) *J. Mater. Chem.*, **14**, 1503.

94 Ostermann, R., Li, D., Yin, Y.D., McCann, J.T., and Xia, Y.N. (2006) *Nano Lett.*, **6**, 1297.

95 Li, D., Ouyang, G., McCann, J.T., and Xia, Y.N. (2005) *Nano Lett.*, **5**, 913.

96 Li, D., Wang, Y.L., and Xia, Y.N. (2003) *Nano Lett.*, **3**, 1167.

97 Li, D., and Xia, Y.N. (2003) *Nano Lett.*, **3**, 555.

98 McCann, J.T., Chen, J.I.L., Li, D., Ye, Z.G., and Xia, Y.A. (2006) *Chem. Phys. Lett.*, **424**, 162.

99 Li, D., and Xia, Y.N. (2004) *Nano Lett.*, **4**, 933.

100 Babel, A., Li, D., Xia, Y.N., and Jenekhe, S.A. (2005) *Macromolecules*, **38**, 4705.

101 Li, D., Babel, A., Jenekhe, S.A., and Xia, Y.N. (2004) *Adv. Mater.*, **16**, 2062.

102 McCann, J.T., Li, D., and Xia, Y.N. (2005) *J. Mater. Chem.*, **15**, 735.

103 Love, J.C., Estroff, L.A., Kriebel, J.K., Nuzzo, R.G., and Whitesides, G.M. (2005) *Chem. Rev.*, **105**, 1103.

104 Hawker, C.J., and Russell, T.P. (2005) *MRS Bull.*, **30**, 952.

105 Ozin, G.A., and Arsenault, A.C. (2005) *Nanochemistry*, RSC Publishing, Cambridge, UK.

106 Burda, C., Chen, X.B., Narayanan, R., and El-Sayed, M.A. (2005) *Chem. Rev.*, **105**, 1025.

107 Murray, C.B., Norris, D.J., and Bawendi, M.G. (1993) *J. Am. Chem. Soc.*, **115**, 8706.

108 Snee, P.T., Chan, Y., Nocera, D.G., and Bawendi, M.G. (2005) *Adv. Mater.*, **17**, 1131.

109 Boatman, E., Lisensky, G.C., and Nordell, K.J. (2005) *J. Chem. Educ.*, **82**, 1697.

110 Peng, X., Wickham, J., and Alivisatos, A.P. (1998) *J. Am. Chem. Soc.*, **120**, 5343.

111 Shim, M., Wang, C., and Guyot-Sionnest, P. (2001) *J. Phys. Chem.*, **105**, 2369.

112 Talapin, D.V., Schevchenko, E.V., Kornowski, A., Gaponik, N., Haase, M., Rogach, A.L., and Weller, H. (2001) *Adv. Mater.*, **13**, 1868.

113 Munro, A.M., Plante, I.J.-L., Ng, M.S., and Ginger, D.S. (2007) *J. Phys. Chem. C*, **111**, 6220.

114 Kittel, C. (1996) *Introduction to Solid State Physics*, 7th edn, John Wiley & Sons, Inc., New York.

115 Bowen Katari, J.E., Colvin, V.L., and Alivisatos, A.P. (1994) *J. Phys. Chem.*, **98**, 4109.

116 Peng, Z.A., and Peng, X. (2001) *J. Am. Chem. Soc.*, **123**, 183.

117 Murray, C.B., Kagan, C.R., and Bawendi, M.G. (2000) *Annu. Rev. Mater. Sci.*, **30**, 545.

118 Sun, B., Marx, E., and Greenham, N.C. (2003) *Nano Lett.*, **3**, 961.

119 Huynh, W.U., Dittmer, J.J., Teclemariam, N., Milliron, D.J., and Alivisatos, A.P. (2003) *Phys. Rev. B*, **67**, 115326.

120 Yu, G., Gao, J., Hummelen, J.C., Wudi, F., and Heeger, A.J. (1995) *Science*, **270**, 1789.

121 Kagan, C.R., Murray, C.B., and Bawendi, M.G. (1996) *Phys. Rev. B*, **54**, 8633.

122 Kagan, C.R. (2003) *Proceedings of the NSF-Conicet Quilmes Nanoscience Workshop* (eds E. Calvo, J. Michl, and C. Kubiak), Quilmes, Provincia de Tucuman, Argentina.

123 Norris, D.J., Bawendi, M.G., and Brus, L.E. (1997) *Molecular Electronics* (eds J. Jortner and M.A. Ratner), Blackwell Science Ltd., Malden, MA, p. 281.

124 Greenham, N.C., Peng, X., and Alivisatos, A.P. (1996) *Phys. Rev. B*, **54**, 17628.

125 Landsberg, P.T., Nussbaumer, H., and Willeke, G. (1993) *J. Appl. Phys.*, **74**, 1451.

126 Weiss, E.A., Chiechi, R.C., Geyer, S.M., Porter, V.J., Bell, D.C., Bawendi, M.G., and Whitesides, G.M. (2008) *J. Am. Chem. Soc.*, **130**, 74.

127 Selmarten, D., Jones, M., Rumbles, G., Yu, P., Nedeljkovic, J., and Shaheen, S. (2005) *J. Phys. Chem. B*, **109**, 15927.

128 Ginger, D.S., and Greenham, N.C. (1999) *Phys. Rev. B*, **59**, 10622.

129 Gowrishankar, V., Miller, N., McGehee, M.D., Misner, M.J., Ryu, D.Y., Russell, T.P., Drockenmuller, E., and Hawker, C.J. (2006) *Thin Solid Films*, **513**, 289.

130 Kim, S.H., Misner, M.J., and Russell, T.P. (2004) *Adv. Mater.*, **16**, 2119.

131 Bosworth, J.K., Paik, M.Y., Ruiz, R., Schwartz, E.L., Huang, J.Q., Ko, A.W., Smilgies, D.M., Black, C.T., and Ober, C.K. (2008) *ACS Nano*, **2**, 1396–1402.

132 Stoykovich, M.P., and Nealey, P.F., (2006) *Mater. Today*, **9**, 20.

133 Stoykovich, M.P., Muller, M., Kim, S.O., Solak, H.H., Edwards, E.W., de Pablo, J.J., and Nealey, P.F. (2005) *Science*, **308**, 1442.

134 Anfinsen, C.B. (1973) *Science*, **181**, 223.

135 Grzybowski, B.A., Radkowski, M., Campbell, C.J., Lee, J.N., and Whitesides, G.M. (2004) *Appl. Phys. Lett.*, **84**, 1798.

136 Novoselov, K.S., Geim, A.K., Morozov, S.V., Jiang, D., Zhang, Y., Dubonos, S.V., Grigorieva, I.V., and Firsov, A.A. (2004) *Science*, **306**, 666.

137 Martinez, A.W., Phillips, S.T., Butte, M.J., and Whitesides, G.M. (2007) *Angew. Chem. Int. Ed.*, **46**, 1318.

138 Martinez, A.W., Phillips, S.T., Carrilho, E., Thomas, S.W., Sindi, H., and Whitesides, G.M. (2008) *Anal. Chem.*, **80**, 3699.

139 Chen, C.S., Breslauer, D.N., Luna, J.I., Grimes, A., Chin, W.C., Leeb, L.P., and Khine, M. (2008) *Lab Chip*, **8**, 622.

140 Grimes, A., Breslauer, D.N., Long, M., Pegan, J., Lee, L.P., and Khine, M. (2008) *Lab Chip*, **8**, 170.

141 Geim, A.K., and Novoselov, K.S. (2007) *Nat. Mater.*, **6**, 183.